Autophagy

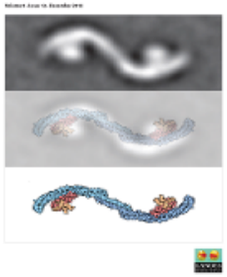

Autophagy

ISSN: 1554-8627 (Print) 1554-8635 (Online) Journal homepage: https://www.tandfonline.com/loi/kaup20

The antimalarial amodiaquine causes autophagic-lysosomal and proliferative blockade sensitizing human melanoma cells to starvation- and chemotherapy-induced cell death

Shuxi Qiao, Shasha Tao, Montserrat Rojo de la Vega, Sophia L Park, Amanda A Vonderfecht, Suesan L Jacobs, Donna D Zhang & Georg T Wondrak

To cite this article: Shuxi Qiao, Shasha Tao, Montserrat Rojo de la Vega, Sophia L Park, Amanda A Vonderfecht, Suesan L Jacobs, Donna D Zhang & Georg T Wondrak (2013) The antimalarial amodiaquine causes autophagic-lysosomal and proliferative blockade sensitizing human melanoma cells to starvation- and chemotherapy-induced cell death, Autophagy, 9:12, 2087-2102, DOI: 10.4161/auto.26506

To link to this article: https://doi.org/10.4161/auto.26506

Published online: 08 Oct 2013.

Autophagy 9:12, 2087–2102; December 2013; © 2013 Landes Bioscience

The antimalarial amodiaquine causes autophagic-lysosomal and proliferative blockade sensitizing human melanoma cells to starvation- and chemotherapy-induced cell death

Shuxi Qiao, Shasha Tao, Montserrat Rojo de la Vega, Sophia L Park, Amanda A Vonderfecht, Suesan L Jacobs, Donna D Zhang, and Georg T Wondrak*

Department of Pharmacology and Toxicology; College of Pharmacy and Arizona Cancer Center; University of Arizona; Tucson, AZ USA

Keywords: malignant melanoma, amodiaquine, chloroquine, autophagy, lysosome, cathepsin, E2F1, CDKN1A

Abbreviations: ACTB, actin, beta; AQ, amodiaquine; ANXA5, annexin AV; BafA, bafilomycin A_1; BECN1, Beclin 1, autophagy related; CCND1, cyclin D1; CDKN1A, cyclin-dependent kinase inhibitor 1A (p21, Cip1); CDDP, cis-dichloro-diamine-platinum (II); CQ, chloroquine; CTSB, cathepsin B; CTSD, cathepsin D, CTSL, cathepsin L; DDIT3, DNA-damage-inducible transcript 3; Doxo, doxorubicin; E2F1, E2F transcription factor 1; EGR1, early growth response 1; GFP, green fluorescent protein; HBSS, Hank's Balanced Salt Solution; HSPA1A, heat shock 70 kDa protein 1A; JC-1, 5,5′,6,6′-tetrachloro-1,1′,3,3′-tetraethylbenzimidazolyl-carbocyanine iodide; LAMP1, lysosomal-associated membrane protein 1; PI, propidium iodide; RB1, retinoblastoma 1; RFP, red fluorescent protein; SDS-PAGE, sodium dodecyl sulfate-polyacrylamide gel electrophoresis; SNCA, synuclein, alpha (non A4 component of amyloid precursor); SQSTM1, sequestosome 1/p62; TEM, transmission electron microscopy; TP53, tumor protein 53

Pharmacological inhibition of autophagic-lysosomal function has recently emerged as a promising strategy for chemotherapeutic intervention targeting cancer cells. Repurposing approved and abandoned non-oncological drugs is an alternative approach to the identification and development of anticancer therapeutics, and antimalarials that target autophagic-lysosomal functions have recently attracted considerable attention as candidates for oncological repurposing. Since cumulative research suggests that dependence on autophagy represents a specific vulnerability of malignant melanoma cells, we screened a focused compound library of antimalarials for antimelanoma activity. Here we report for the first time that amodiaquine (AQ), a clinical 4-aminoquinoline antimalarial with unexplored cancer-directed chemotherapeutic potential, causes autophagic-lysosomal and proliferative blockade in melanoma cells that surpasses that of its parent compound chloroquine. Monitoring an established set of protein markers (LAMP1, LC3-II, SQSTM1) and cell ultrastructural changes detected by electron microscopy, we observed that AQ treatment caused autophagic-lysosomal blockade in malignant A375 melanoma cells, a finding substantiated by detection of rapid inactivation of lysosomal cathepsins (CTSB, CTSL, CTSD). AQ-treatment was associated with early induction of energy crisis (ATP depletion) and sensitized melanoma cells to either starvation- or chemotherapeutic agent-induced cell death. AQ displayed potent antiproliferative effects, and gene expression array analysis revealed changes at the mRNA (*CDKN1A*, *E2F1*) and protein level (TP53, CDKN1A, CCND1, phospho-RB1 [Ser 780]/[Ser 807/811], E2F1) consistent with the observed proliferative blockade in S-phase. Taken together, our data suggest that the clinical antimalarial AQ is a promising candidate for repurposing efforts that aim at targeting autophagic-lysosomal function and proliferative control in malignant melanoma cells.

Introduction

Autophagy is an evolutionarily conserved, intracellular catabolic pathway that serves survival functions by maintaining cellular homeostasis under adverse conditions such as nutrient deprivation and accumulation of misfolded proteins or damaged organelles.[1-3] Dysregulation of autophagy has been implicated in a broad range of human pathologies including neurodegeneration and cancer,[4,5] and pathological alterations of autophagic-lysosomal function can also occur in response to exposure to environmental toxicants such as arsenic and solar UV radiation.[6-8] Recent evidence suggests that cancer cells may harness autophagic pathways as an adaptation to conditions associated with the tumor microenvironment including increased levels of oxidative and

*Correspondence to: Georg T Wondrak; Email: wondrak@pharmacy.arizona.edu
Submitted: 05/17/2013; Revised: 09/09/2013; Accepted: 09/16/2013
http://dx.doi.org/10.4161/auto.26506

proteotoxic stress, hypoxia, and energy crisis.[5,9,10] Autophagy also occurs in response to exposure to major classes of chemotherapeutic agents (e.g., cisplatin and doxorubicin [Doxo]), a process thought to contribute to cancer cell chemoresistance.[5,11,12] Therefore, pharmacological inhibition of autophagic-lysosomal function has recently emerged as a promising strategy for therapeutic intervention that may preferentially target cancer cells without compromising viability of normal cells.[4,5,9,13-15]

Repurposing approved and abandoned non-oncological drugs is an alternative developmental strategy for the identification of anticancer therapeutics, and antimalarials that potentially undermine autophagic-lysosomal functions have recently attracted considerable attention as promising candidates for oncological repurposing.[4,16,17] Since all autophagic pathways (including macroautophagy, microphagy, and chaperone-mediated autophagy) converge on lysosomal fusion followed by enzymatic degradation irrespective of the specific mechanism employed for cargo selection and trafficking, members of the lysosomotropic 8-aminoquinoline (e.g., primaquine, pamaquine), 4-aminoquinoline (e.g., chloroquine [CQ], hydroxychloroquine), and quinoline (e.g., mefloquine) classes of antimalarials that disrupt lysosomal pH control and function have been examined as experimental (preclinical) and investigational (clinical) cancer therapeutics.[4,14,18-23] Indeed, CQ and hydroxychloroquine are currently undergoing evaluation in numerous oncological clinical trials that examine potentiation of therapeutic efficacy by combining cytotoxic chemotherapeutics with autophagic-lysosomal antagonists.[21] However, limited efficacy and systemic toxicity associated with these prototype agents create an urgent need for the identification and development of improved therapeutics that target autophagic-lysosomal function in cancer cells.[5,9,24]

Melanoma is a malignant melanocyte-derived tumor causing the majority of deaths attributed to skin cancer.[25,26] Despite recent progress in the design of targeted therapies such as the V600E-mutation directed BRAF-inhibitor vemurafenib, efficacy of chemotherapeutic intervention directed against the metastatic stage of the disease remains limited, and identification and development of improved molecular agents targeting malignant melanoma cells remain important goals of current research.[27] Cumulative evidence suggests the involvement of autophagic dysregulation in melanomagenesis, and the emerging role of autophagy as a prognostic factor and therapeutic target in melanoma has been substantiated recently.[15,28-31] Consistent with this hypothesis, the efficacy of cisplatin chemotherapeutic intervention targeting melanoma can be potentiated by inhibitors of autophagy, and leucine deprivation combined with pharmacological suppression of autophagy shows therapeutic efficacy in a murine xenograft model of the human disease.[10,32]

Recently, we have screened a compound library of clinical antimalarials for antimelanoma activity, identifying the endoperoxide-based redox antimalarial dihydroartemisinin and other members of the artemisinin-class as potent inducers of melanoma cell apoptosis.[33,34] As part of our screening efforts we also focused on amodiaquine (AQ; 4-[(7-chloroquinolin-4-yl)amino]-2-[(diethylamino)methyl]phenol CAS#: 86-42-0; chemical structure: **Fig. 1A**), a member of the lysosomotropic 4-aminoquinoline class of antimalarials used worldwide in combination with artemisinin-drugs.[35,36] AQ displays potent plasmodium-directed activity that may surpass that of its parent compound CQ, but its potential cancer cell-directed activities have remained unexplored. Here we report for the first time that AQ targets malignant melanoma cells with pronounced induction of autophagic-lysosomal and proliferative blockade causing sensitization to starvation- and chemotherapeutic-induced cell death.

Results

Amodiaquine causes morphological alterations in human malignant A375 melanoma cells consistent with lysosomal impairment

First, AQ-induced morphological changes were examined in human A375 melanoma cells using light microscopy (**Fig. 1B**) and transmission electron microscopy (TEM; **Fig. 1C and D**). Visualization by light microscopy revealed a distinct accumulation of vacuole structures with predominantly perinuclear localization within 24 h AQ exposure, not observed in untreated control cells (**Fig. 1B**). Subsequent TEM analysis (magnification 2,650 and 25,000 fold) (**Fig. 1C and D**) of AQ-exposed melanoma cells indicated the pronounced formation of large (0.5–2 μm diameter), multivesicular single membrane-enclosed structures containing electron-dense osmiophilic inclusions, an observation indicative of lysosomal expansion and lipofuscin accumulation, not observed in untreated control cells.[7,37,38] In contrast, no accumulation of double-membrane-enclosed small vesicles that would be indicative of increased autophagosome formation was observed in response to AQ treatment. Time-course analysis demonstrated that formation of osmiophilic, multivesicular structures in AQ-treated melanoma cells could be observed within 6 h, reaching a plateau at 18- to 24 h exposure time (**Fig. 1D**).

Amodiaquine causes autophagic-lysosomal blockade in human malignant A375 melanoma cells

Next, immunoblot analysis demonstrated AQ-induced accumulation of lysosomal-associated membrane protein 1 (LAMP1) indicative of lysosomal expansion as already suggested by TEM visualization (**Fig. 2A**).[7,39] In parallel, massive accumulation of LC3-II occurred in response to AQ exposure in a dose-dependent manner and could be observed at concentrations as low as 1 μM. LC3, the mammalian homolog of yeast Atg8, is an essential factor for autophagosome formation that relocalizes to and participates in the formation of the autophagosomal membrane after C-terminal proteolytic processing and posttranslational phospholipid-conjugation. Therefore, after relocalization of LC3-I to newly formed vesicles a more rapidly migrating lipidated form (LC3-II) is detectable by SDS-PAGE (**Fig. 2A**).[40]

Strikingly, pronounced accumulation of SQSTM1/p62 (sequestosome 1), an autophagic cargo receptor and substrate that undergoes depletion upon autophagy induction, occurred at the protein level.[7,41-43] Similar accumulation occurred with SNCA (α-synuclein), another autophagic substrate protein that accumulates as a consequence of blocked autophagic-lysosomal flux.[7,44,45] In contrast, BECN1 (Beclin 1), a critical component of

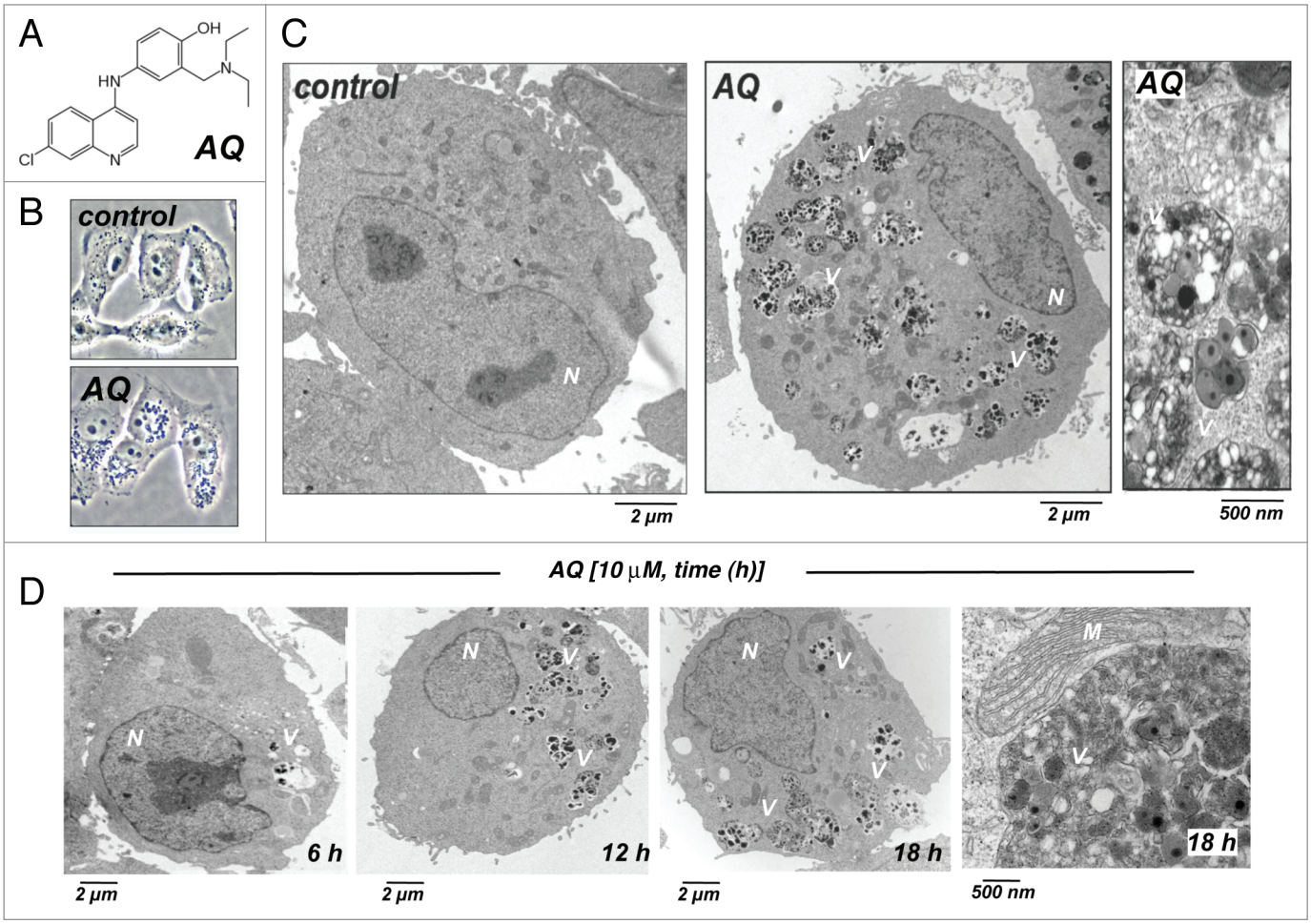

Figure 1. Amodiaquine-induced morphological changes in human malignant A375 melanoma cells. (**A**) Chemical structure of AQ. (**B**) Cells were exposed to AQ (10 μM, 24 h) or remained untreated (control). Visualization by light microscopy (upper panel: control; bottom panel: AQ). (**C**) Transmission electron microscopy. left: control; middle: AQ (10 μM, 24 h; 2,650-fold direct magnification); right: AQ (10 μM, 24 h; 25,000-fold direct magnification). (**D**) Transmission electron microscopy; time-course analysis (AQ, 10 μM, 6–18 h; 2,650-fold direct magnification); right panel: AQ (10 μM, 18 h; 25,000-fold direct magnification); M, mitochondrion; N, nucleus; V, single membrane-enclosed osmiophilic multivesicles.

the class III PtdIns 3-kinase complex involved in autophagosome formation, remained unchanged at the protein (**Fig. 2A**) and mRNA (data not shown) levels.[46] Since it has been shown earlier that the aminophenol-moiety contained in AQ (but not CQ) can cause protein modification (haptenization) we also explored the possibility that AQ may cause covalent protein adduction in malignant melanoma cells.[47,48] Using a monoclonal antibody (6D10) employed for the immunodetection of AQ-adducted plasma protein in malaria patients, we detected the accumulation of AQ-modified proteins (35- to 55-kDa molecular mass range) in melanoma cells exposed to AQ (20 μM, 24 h; **Fig. 2A**). However, identity of adducted target proteins and causative involvement of protein adduction in AQ-induced autophagic-lysosomal impairment remain undefined at this point.

Consistent with TEM-visualization of osmiophilic vesicles (**Fig. 1C and D**), A375 cells displayed increased lipofuscin accumulation as evidenced by flow cytometric detection of autofluorescent intracellular material that formed upon prolonged AQ exposure (24–48 h; **Fig. 2B**), changes indicative of impaired autophagic-lysosomal function as described before.[7,37,38] Importantly, similar changes affecting LAMP1, LC3-II, and SQSTM1 were observed in human G361 metastatic melanoma cells exposed to low micromolar concentrations of AQ (**Fig. 2C**).

After demonstrating accumulation of autophagy substrates and lysosomal marker proteins (LC3-II, SQSTM1, SNCA, LAMP1) we gathered further mechanistic evidence in support of AQ-induced autophagic-lysosomal blockade by monitoring LC3 puncta formation in A375 melanoma cells.[49] To this end, cells transfected with a tandem reporter construct (RFP-GFP-LC3) were exposed to AQ (10 μM, 24 h) followed by assessment of GFP-LC3 and RFP-LC3 puncta colocalization (**Fig. 2D**).[6,49] GFP-fluorescence is quenched in acidic environments (such as that encountered in the autolysosome), whereas RFP is more stable under acidic conditions. Therefore, colocalization of both GFP and RFP fluorescence (yellow puncta in a merged image) indicates either autophagosomal localization (upstream of fusion with the acidic lysosome) or autolysosomal localization (i.e., in autolysosomes with disrupted acidification). Indeed, exposure to

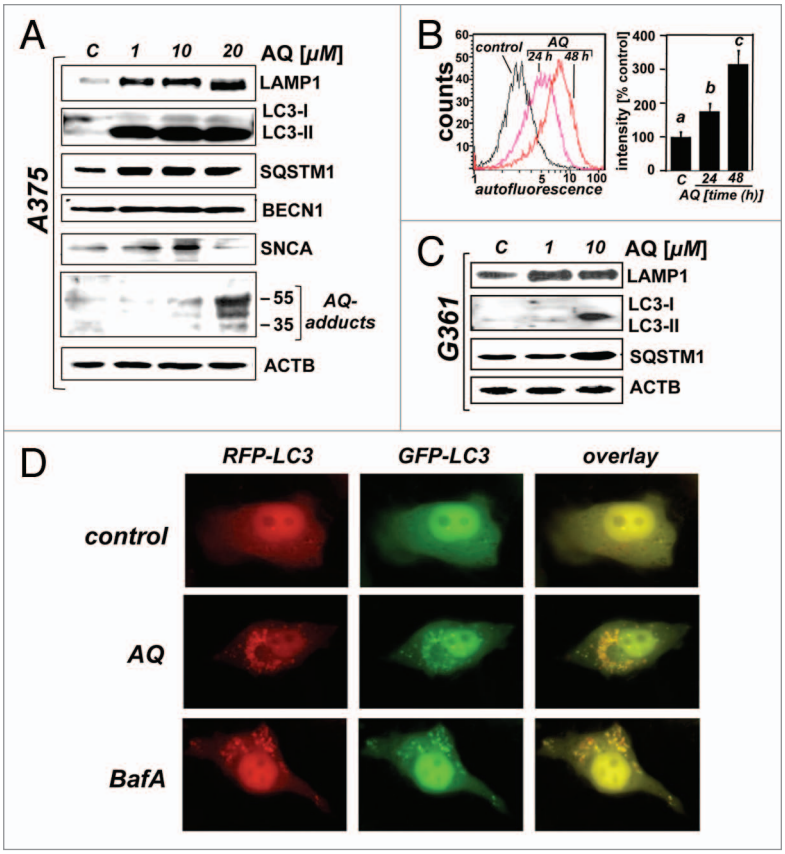

Figure 2. Amodiaquine-induced autophagic-lysosomal alterations in human malignant melanoma cells. (**A**) After exposure of A375 cells to AQ (1–20 μM; 24 h), modulation of autophagic-lysosomal proteins (LC3-I/-II, SQSTM1, BECN1, LAMP1, SNCA) was detected by immunoblot analysis (loading control: ACTB). Protein adduction of unidentified target proteins was detected using an AQ-directed monoclonal antibody. (**B**) Cellular autofluorescence as detected by flow cytometric analysis. After exposure to AQ (10 μM, 24–48 h), autofluorescence intensity of A375 cells was quantified by flow cytometry (left panel: histogram representative of three similar repeats; right panel: bar graph summarizing data from three independent repeats [n = 3, mean ± S.D.; $P < 0.05$]). (**C**) AQ-induced changes as examined in G361 metastatic melanoma cells (1–10 μM, 24 h) detected as in (**A**). (**D**) Autophagic flux analysis using the RFP-GFP-LC3 puncta formation assay. After transfection using a tandem reporter construct (RFP-GFP-LC3) cells were exposed to AQ (10 μM, 24 h), and colocalization of GFP-LC3 and RFP-LC3 puncta was examined using fluorescence microscopy. Dual fluorophore-labeled LC3 transfectants appear yellow upon colocalization. A similar fluorescence pattern (accumulation of yellow fluorescent puncta) was observed in response to the lysosomal proton pump inhibitor BafA (100 nM, ≤ 24 h).

AQ caused pronounced formation of LC3 puncta that displayed both green and red fluorescence intensity producing a yellow overlay, consistent with accumulation of autolysosomes that display impaired acidification. Furthermore, control cells exposed to bafilomycin A_1 (BafA, a standard inhibitor of lysosomal acidification and substrate degradation that impairs autophagosome-lysosome fusion[50]) displayed an LC3-fluorescence pattern (puncta formation with yellow overlay) that mimicked that induced by AQ treatment. Moreover, consistent with the published literature on lysosomotropic agents, fluorescence imaging using the pH sensitive lysosomal probe LysoSensor™ Green DND-189 revealed a similar pattern of impaired lysosomal acidification resulting in rapid loss of pH control in response to treatment with either BafA or AQ (data not shown).[51]

In order to gain further insight into the mechanism of AQ-induced autophagic-lysosomal alterations, an LC3 turnover assay employing BafA cotreatment was performed (**Fig. 3A**).[49] In this assay, we assessed AQ-induced LC3-II accumulation in the presence or absence of the lysosomal inhibitor BafA. As observed above (**Fig. 2A**), AQ treatment caused an increase of LC3-II levels within 4–8 h exposure time. Importantly, if AQ exposure occurred in the presence of BafA, AQ-induced upregulation of LC3-II levels was not potentiated, an observation most consistent with an autophagic-lysosomal blockade of LC3-II degradation at the autolysosomal level.

In support of a direct impairment of lysosomal function by AQ treatment, pronounced inhibition of cathepsin enzymatic activity was detected in A375 cells that occurred in a dose- and time-dependent manner (1–20 μM, 1–24 h; **Fig. 3B**). AQ treatment caused pronounced enzyme inactivation of both cysteine- (CTSB [cathepsin B] and CTSL [cathepsin L]) and aspartate-dependent (CTSD [cathepsin D]) cathepsins, consistent with a global impairment of lysosomal function by this lysosomotropic 4-aminoquinoline-derivative. Remarkably, within only 1 h AQ exposure time, CTSB enzymatic activity was already reduced by almost 25% diminishing further over the next 12 h, with only approximately 30% residual activity detectable. This inhibitory effect is in accordance with the documented activity of lysosomotropic antimalarials (including CQ and AQ) that disrupt the acidic food vacuole of the plasmodium parasite and also compromise mammalian cell lysosomal function through alkalinization and membrane destabilization.[52,53] Interestingly, recent evidence indicates that lysosomal cathepsins including CTSB and CTSD are involved in LC3-II proteolytic turnover and that pharmacological inhibition of CTSB causes accumulation of LC3-II, supporting the hypothesis that cathepsin inactivation is the causative factor underlying massive accumulation of LC3-II as observed in AQ-exposed A375 melanoma cells (**Fig. 2A**).[54,55]

Importantly, inhibition of CTSB and CTSL activity by AQ treatment was also observable in other melanoma cell lines including G361 (**Fig. 3C**). However, CTSD activity remained undiminished in G361 cells exposed to AQ, indicating a differential sensitivity of cysteine-dependent (CTSB/L) vs. aspartate-dependent (CTSD) cathepsins in G361 cells, a phenomenon that remains poorly understood at this time.

AQ induces energy crisis and sensitizes malignant melanoma cells to starvation- and chemotherapeutic-induced death

Next, we examined AQ modulation of melanoma cell vulnerability to starvation and chemotherapeutic intervention (**Fig. 4**). In untreated control cells exposed to Hank's Balanced

Salt Solution (HBSS, causing serum and amino acid starvation) for up to 24 h, pronounced depletion of the autophagy substrate SQSTM1 was observed, an observation in accordance with the established stimulatory effect of starvation on autophagic activity (**Fig. 4A**, upper panel). This starvation-induced depletion of SQSTM1 was completely suppressed by AQ co-treatment suggesting that AQ-blockade of autophagic-lysosomal function interferes with starvation-induced degradation of autophagy substrates (**Fig. 4A**, bottom panel).

We also observed that AQ-exposed melanoma cells displayed early energy crisis as evident from significant depletion of cellular total ATP levels that occurred as early as within 1 h treatment (**Fig. 4B**), consistent with earlier reports indicating that aminoquinoline-antimalarials may compromise mitochondrial function and transmembrane potential.[51,56] Consistent with an induction of energy crisis due to impairment of mitochondrial function,[57-59] flow cytometric analysis using the sensor dye JC-1 revealed a moderate yet significant decrease in mitochondrial transmembrane potential ($\Delta\psi m$) observable at early time points (10 μM, 6 h; **Fig. 4C**: top panels: bivariate analysis), where AQ treatment diminished JC-1 red fluorescence intensity (indicative of fully polarized mitochondria) by approximately 25.0% (control: 1382.82 ± 76.40; AQ: 1056.85 ± 34.68; n = 3; **Fig. 4C**; bottom panel). Importantly, even upon longer exposure to AQ no further reduction in $\Delta\psi m$ was observed (data not shown), and cells maintained full viability (10 μM AQ, 48 h; **Fig. 4D**). Even though neither starvation nor extended exposure to AQ (10 μM, 48 h) diminished cellular viability if administered separately (**Fig. 4D**), pronounced induction of cell death occurred in response to combination treatment (starvation plus AQ exposure). These data strongly suggest that AQ compromises mitochondrial function and blocks starvation-induced autophagic-lysosomal adaptations thereby sensitizing melanoma cells to the cytotoxic metabolic stress imposed by prolonged starvation.

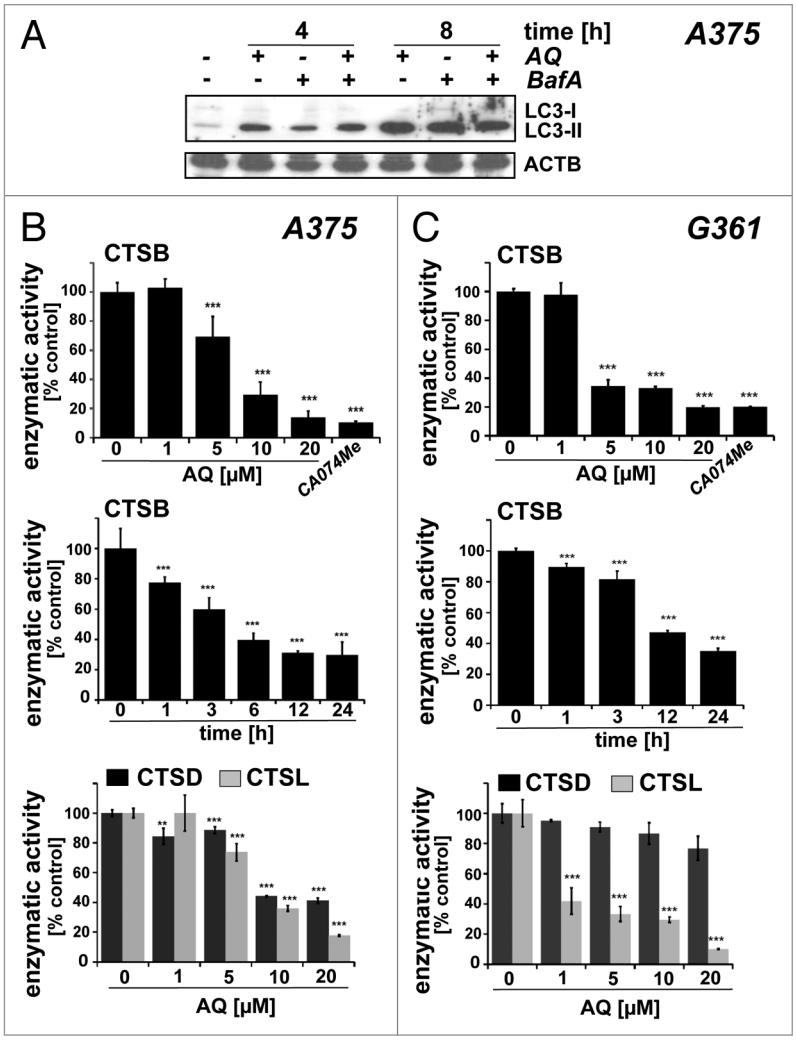

Figure 3. Amodiaquine-induced loss of cathepsin enzymatic activity in human malignant melanoma cells. (**A**) Immunoblot detection of LC3-II in A375 cells left untreated (lane 1), exposed to BafA only (100 nM; 4 or 8 h; lanes 3, 6), or exposed to AQ (10 μM) in the absence (lanes 2 and 5) or presence of BafA (lanes 4 and 7). (**B and C**) Loss of cathepsin-specific enzymatic activity in A375 (**B**) and G361 cells (**C**) exposed to AQ (1–20 μM, ≤ 24 h) was detected using a fluorimetric assay. Top panels: CTSB, dose response (24 h); middle panels: CTSB, time course (10 μM); bottom panels: CTSD and CTSL, dose response (24 h). Treatment with the CTSB/L inhibitor CA074Me (20 μM) served as a positive control (n = 3, mean ± S.D.; $P < 0.05$).

Cumulative evidence suggests a role of autophagic dysregulation in cancer cell resistance to chemotherapeutic agents.[5,11,12] Based on our observation that AQ is a potent inhibitor of autophagic-lysosomal function we therefore tested the hypothesis that AQ may sensitize melanoma cells to the cytotoxic action of standard chemotherapeutics. Indeed, we observed that cytotoxicity of specific chemotherapeutics (CDDP, Doxo) was strongly potentiated upon co-exposure with AQ employed at concentrations that do not impair viability of A375 melanoma cells if used as single treatment (**Fig. 4E and F**). Specifically, when cells were exposed to the combined action of CDDP and AQ, the fraction of dead cells increased from approximately 20.0% (CDDP only) to over 70.0% (CDDP plus AQ; **Fig. 4E**). Moreover, when cells were exposed to the combined action of Doxo and AQ, the fraction of dead cells increased from approximately 5.0% (Doxo only) to over 90.0% (Doxo plus AQ; **Fig. 4F**).

Gene expression array analysis reveals an AQ-induced proliferative blockade in A375 melanoma cells

To gain further mechanistic insight into the molecular events underlying antimelanoma activity of AQ, we performed gene expression array analysis. To this end, modulation of gene expression in response to AQ exposure (25 μM, 24 h), vs. control was assessed using a PCR-based expression array system. Out of 168 cell stress and autophagy-related genes contained on the combined array, 25 genes displayed AQ-induced expression changes at the mRNA level by at least 2-fold over untreated control cells (**Fig. 5A and B**). Strikingly, AQ treatment caused pronounced

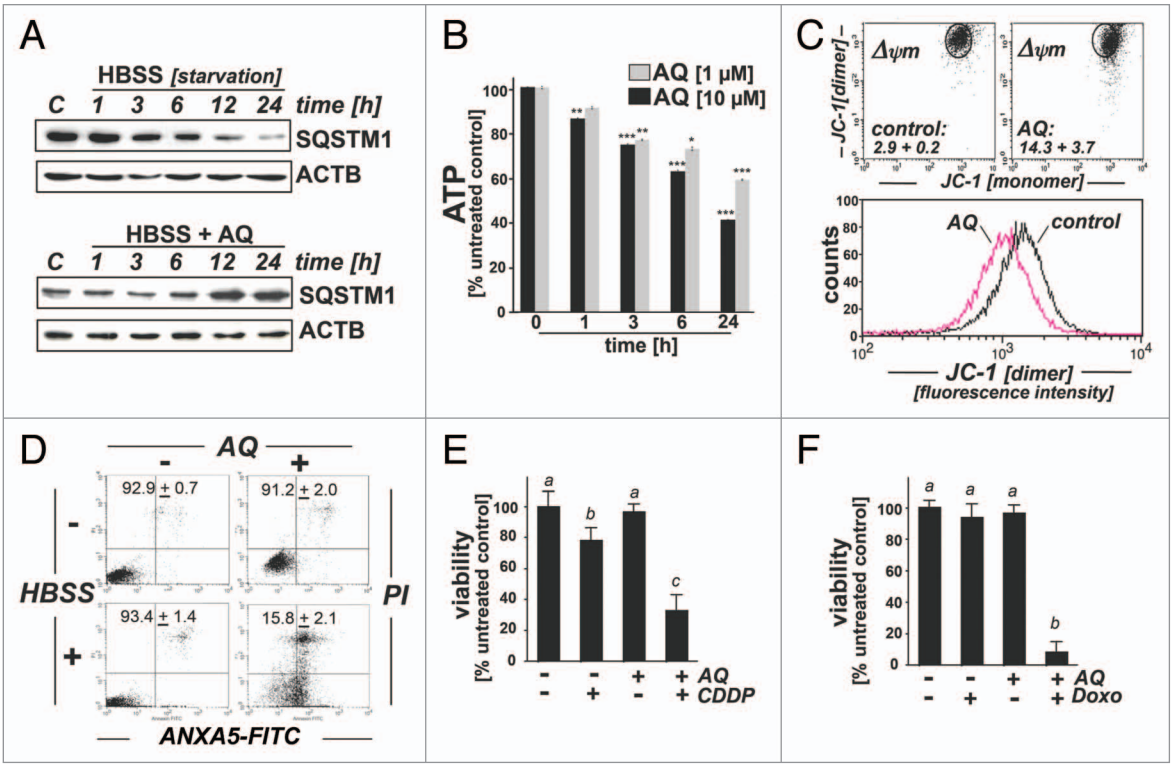

Figure 4. Amodiaquine causes rapid ATP depletion and sensitization to starvation- and chemotherapeutic-induced cell death. (**A**) AQ modulation of starvation-induced SQSTM1 depletion. A375 melanoma cells were cultured In HBSS in the presence or absence of AQ (10 μM, 1–24 h). Protein levels of SQSTM1 were determined by immunoblot analysis using ACTB as a loading control. (**B**) Early cellular ATP depletion induced by AQ exposure (1 and 10 μM, ≤ 24 h). Data are expressed as % of untreated controls (mean ± S.D.; n = 3). (**C**) Alteration of mitochondrial transmembrane potential (Δψm) in response to AQ (10 μM, 6 h) as assessed by bivariate flow cytometric analysis of JC-1-stained cells. The upper two panels display one representative experiment of three similar repeats, and numbers indicate cells with impaired Δψm (in percent of total gated cells) detected outside the circle (mean ± SD, n = 3). Lower panel displays AQ-induced alteration of JC-1 red fluorescence (polarized mitochondria, detector FL-2; 1 representative experiment of 3 similar repeats). (**D**) Cell viability as determined by flow cytometric analysis of ANXA5-FITC/PI staining in cells cultured in HBSS or standard medium in the presence or absence of AQ (10 μM, 48 h). The numbers indicate viable ($ANXA5^-/PI^-$) in percent of total gated cells (mean ± S.D.; n = 3). (**E and F**) Chemosensitization by AQ was examined in A375 cells exposed to the combined action of cisplatin (CPPD, 20 μM; 24 h [**D**]) or doxorubicin (Doxo, 10 nM; 24 h; [**E**]) with or without AQ (10 μM, 24 h). Cell viability was analyzed by flow cytometry. The bar graph summarizes data from three repeats (n = 3, mean ± S.D.). Data were analyzed employing one-way analysis of variance (ANOVA) with Tukey's post hoc test. Means without a common letter differ from each other ($P < 0.05$).

modulation of gene expression antagonizing cell cycle progression. *E2F1*, the gene encoding the transcription factor and master regulator of G_1/S cell cycle transition, E2F1, displayed the highest negative expression differential (6.7-fold downregulation) elicited by AQ. Conversely, expression of *CDKN1A*, the TP53-controlled gene encoding CDKN1A (cyclin-dependent kinase inhibitor 1A [p21, Cip1]), a negative regulator of cell cycle progression causing G_1, G_2, or S-phase arrest,[60] was upregulated significantly (4.2-fold). Subsequent immunoblot analysis confirmed *E2F1* and *CDKN1A* expression changes at the protein level (E2F1, CDKN1A; **Fig. 6A and B**), and a dose response relationship of *CDKN1A* mRNA upregulation was established (**Fig. 6C**).

AQ treatment also caused negative modulation of a broad array of genes encoding heat shock response proteins (*HSPA8*, *HSPA1A*, *HSP90AA1*, *HSPCA*, *HSPA2*, *HSPA1L*, *DNAJA1*, *CRYAB*),[61] and a dose response relationship of *HSPA1A* mRNA downregulation was established (**Fig. 6C**). AQ-induced suppression of heat shock response-encoding genes was also observed at the protein level (HSPA1A, HSP90AA1; **Fig. 6A and B**). Pharmacological downregulation of heat shock response gene expression is expected to increase proteotoxic stress, particularly in cancer cells constitutively exposed to a high unfolded protein burden.[62,63] Indeed, consistent with the suppression of heat shock response gene expression by AQ, array analysis indicated transcriptional upregulation of the ER stress response gene *DDIT3* (6.1 fold) encoding a transcription factor (also known as CHOP/GADD153), a common marker of proteotoxic stress.[64]

In addition, upregulation of other genes responsive to various types of cytotoxic stress was observed in AQ-treated A375 cells including *GADD45A* (encoding growth arrest and DNA-damage-inducible, α, a TP53-regulated DNA damage inducible stress sensor), *EGR1* (encoding early growth response 1, an oxidative stress-sensitive transcription factor), and *TP53* (encoding tumor protein p53, a genotoxic stress- and general stress-responsive tumor suppressor and transcription factor). Importantly, pronounced *TP53* upregulation was also observed at the protein level (TP53; **Fig. 6A**), and upregulation of the TP53 target gene *GDF15* (encoding growth differentiation factor

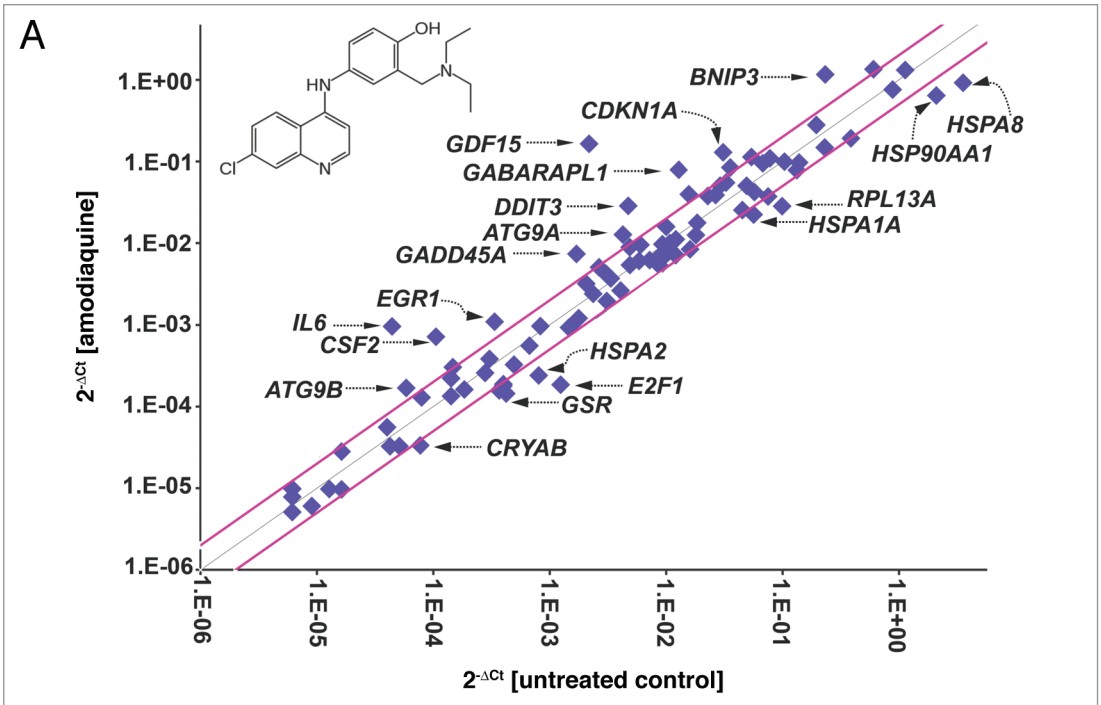

B

gene symbol (accession number)	gene name	fold change (p < 0.05)
GDF 15 (NM_004864)	Growth differentiation factor 15	75.6
IL6 (NM_000600)	Interleukin 6 (interferon, beta 2)	21.6
CSF2 (NM_000758)	Colony stimulating factor 2 (granulocyte-macrophage)	6.8
GABARAPL1 (NM_031412)	GABA(A) receptor-associated protein like 1	6.1
DDIT3 (NM_004083)	DNA-damage-inducible transcript 3	6.1
BNIP3 (NM_004052)	BCL2/adenovirus E1B 19kDa interacting protein 3	5.0
GADD45A (NM_001924)	Growth arrest and DNA-damage-inducible, alpha	4.4
CDKN1A (NM_000389)	Cyclin-dependent kinase inhibitor 1A (p21, Cip1)	4.2
BCL2L1 (NM_138578)	BCL2-like 1	3.9
EGR1 (NM_001964)	Early growth response 1	3.3
ATG9A (NM_024085)	ATG9 autophagy related 9 homolog A (S. cerevisiae)	3.0
ATG9B (NM_173681)	ATG9 autophagy related 9 homolog B (S. cerevisiae)	3.0
ATG4D (NM_032885)	ATG4 autophagy related 4 homolog D (S. cerevisiae)	2.5
TP53 (NM_000546)	Tumor protein p53	2.4
LAMP1 (NM_005561)	Lysosomal-associated membrane protein 1	2.1
DNAJA1 (NM_001539)	DnaJ (Hsp40) homolog, subfamily A, member 1	-2.0
HSPA1L (NM_005527)	Heat shock 70kDa protein 1-like	-2.2
GSR (NM_000637)	Glutathione reductase	-2.3
CRYAB (NM_001885)	Crystallin, alpha B	-2.3
HSPA1A (NM_005345)	Heat shock 70kDa protein 1A	-2.5
HSPA2 (NM_021979)	Heat shock 70kDa protein 2	-2.9
HSP90AA1 (NM_001017963)	Heat shock protein 90kDa alpha (cytosolic), class A member 1	-3.3
RPL13A (NM_012423)	Ribosomal protein L13a	-3.5
HSPA8 (NM_006597)	Heat shock 70kDa protein 8	-3.9
E2F1 (NM_005225)	E2F transcription factor 1	-6.7

Figure 5. Gene expression array analysis performed in A375 melanoma cells exposed to amodiaquine. Gene expression in response to AQ (25 μM, 24 h) was analyzed using the Human Autophagy RT²Profiler™ and the Human Stress and Toxicity RT²Profiler™ PCR Expression Arrays. (**A**) The scatter blot depicts differential gene expression (AQ vs. untreated control). Upper and lower lines: cut-off indicating 2-fold up- or downregulated expression, respectively. Arrays were performed in 3 independent repeats and analyzed using the two-sided Student *t* test. (**B**) The table summarizes expression changes by at least 2-fold ($P < 0.05$).

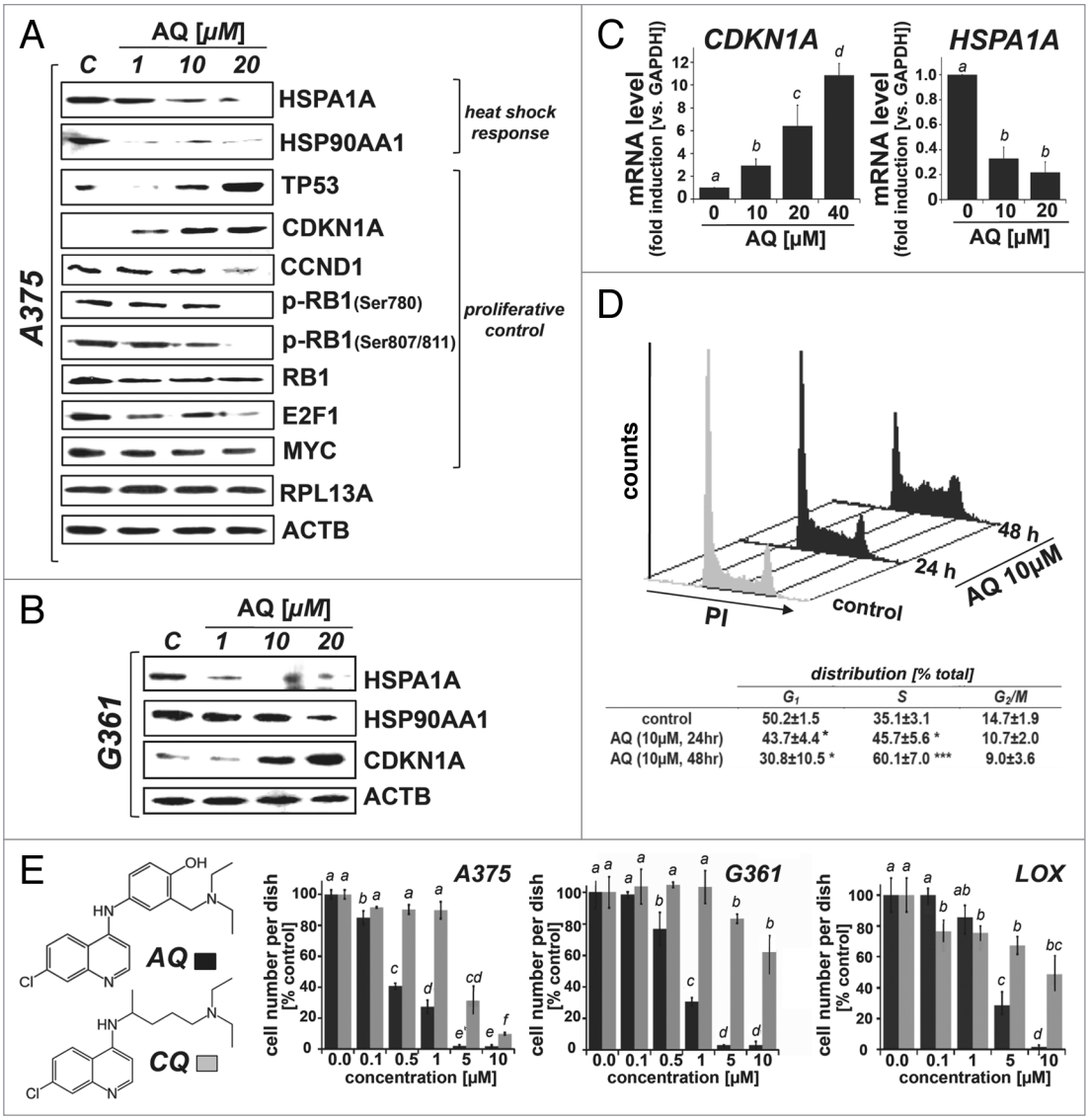

Figure 6. Amodiaquine treatment modulates cell cycle regulators (CDKN1A, RB1 [Ser780; Ser807/811], CCND1, E2F1) causing inhibition of proliferation and S phase cell cycle arrest. (**A**) Immunoblot detection of AQ-induced (≤ 20 μM; 24 h) expression changes affecting heat shock proteins and major cell cycle regulators in A375 cells (loading control: ACTB). (**B**) Immunoblot analysis of AQ-induced expression changes in G361 melanoma cells treated as in (**A**). (**C**) *CDKN1A* and *HSPA1A* mRNA levels in A375 cells exposed to AQ (10, 20, 40 μM; 24 h) were determined by real time RT-PCR analysis (mean ± S.D., n = 3). (**D**) Representative histogram depicting cell cycle distribution after treatment with AQ (10 μM, ≤ 48 h). After treatment for the indicated time periods, cells were stained with PI and analyzed by flow cytometry. The data indicate the percentage of cells in each phase of the cell cycle. The table summarizes results from 3 independent repeat experiments (mean ± SD [n = 3]; *$P < 0.05$; **$P < 0.01$; ***$P < 0.001$). (**E**) Dose-response relationship of AQ or CQ-induced inhibition of proliferation in malignant melanoma cell lines (A375, G361, LOX). After 72 h exposure to increasing concentrations of AQ or CQ, number of adherent cells on the dish was determined by cell counting and expressed as % of untreated control (means ± S.D.; n = 3)

15, a member of the transforming growth factor β superfamily) was observed.[65] Finally, AQ treatment also caused expression changes affecting genes involved in inflammatory signaling (*IL6* encoding interleukin 6, [interferon β 2]; *CSF2* encoding colony stimulating factor [granulocyte-macrophage]) and autophagic regulation (autophagy-related genes *ATG9A*, *ATG9B*, *ATG4D; GABARAPL1*, *BNIP3*), but none of these changes were substantiated at the protein level.

Antiproliferative activity of AQ is associated with S phase cell cycle arrest and modulation of G_1/S cell cycle regulators

Flow cytometric analysis revealed that AQ exposure imposed pronounced alterations in cell cycle distribution. Specifically, continuous exposure of A375 cells to AQ (10 μM, 48 h) caused a statistically significant increase in S-phase fraction that was accompanied by a decrease of cells in G_1 and G_2/M phase (**Fig. 6D**). Specifically, the fraction of cells in S phase increased from approximately 35% to 60% upon treatment with AQ (10 μM, 48 h), accompanied by pronounced depletion of cells in G_1 and G_2/M. Further experiments employing a panel of cultured human melanoma cell lines (A375, G361, LOX) confirmed that AQ caused pronounced antiproliferative activity at

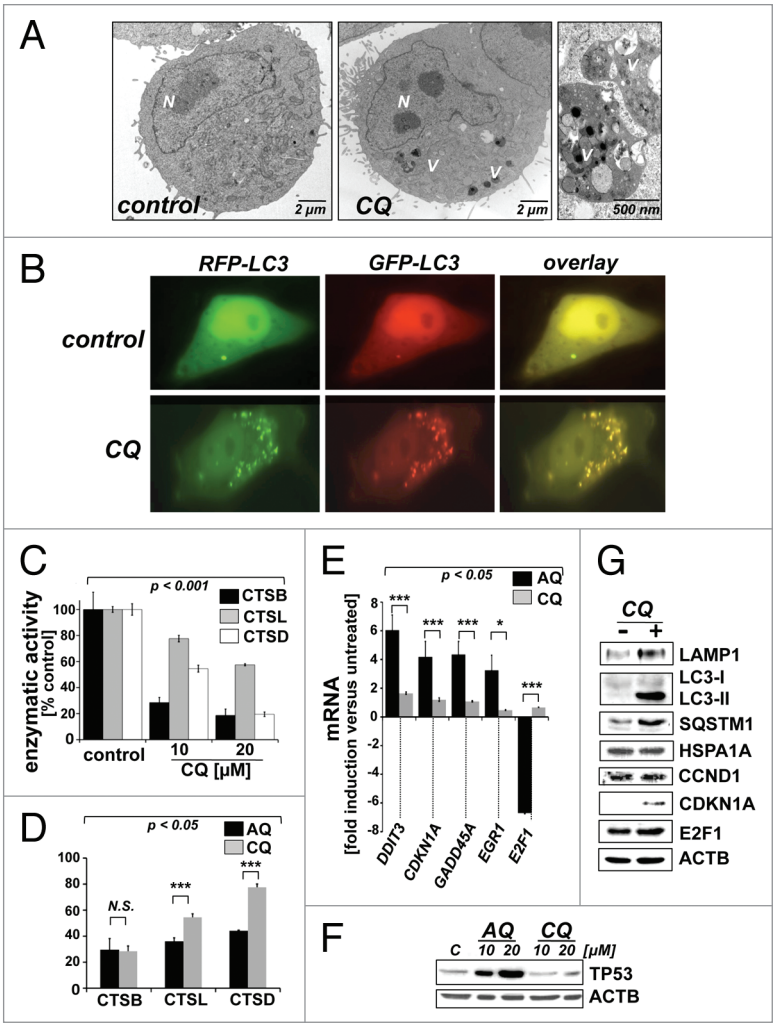

Figure 7. Comparative analysis of chloroquine- vs. amodiaquine-induced antiproliferative effects. Cells were exposed to CQ (10 μM, 24 h) or remained untreated (control). (**A**) Visualization by transmission electron microscopy [control; CQ, (2,650-fold direct magnification); CQ (25,000-fold direct magnification)]; M, mitochondrion; N, nucleus; V, single membrane-enclosed osmiophilic multivesicles). (**B**) Autophagic flux analysis using the RFP-GFP-LC3 puncta formation assay. After transfection using a tandem reporter construct (RFP-GFP-LC3) cells were exposed to AQ (10 μM, 24 h), and colocalization of GFP-LC3 and RFP-LC3 puncta was examined using fluorescence microscopy. Dual fluorophore-labeled LC3 transfectants appear yellow originating from overlapping green and red fluorescence, consistent with accumulation of autolysosomes displaying impaired acidification. (**C**) Loss of cathepsin enzymatic activity (CTSB, CTSL, CTSD) in A375 cells exposed to AQ (≤ 20 μM, 24 h) detected as described above. (**D**) Comparative potency of AQ vs. CQ (10 μM, 24 h) inhibiting CTSB, CTSL, and CTSD enzymatic activity. (**E**) AQ- vs. CQ-induced (≤ 25 μM, 24 h) expression changes at the mRNA level in A375 melanoma cells. (**F**) Immunoblot detection of CQ- and AQ-induced (≤ 20 μM, 24 h) expression changes of TP53 protein. (**G**) Immunoblot detection of CQ-induced expression changes at the protein level in A375 melanoma cells.

submicromolar concentrations (A375: IC_{50} = 0.32 ± 0.12 μM; G361: IC_{50} = 0.71 ± 0.16 μM; LOX: IC_{50} = 2.60 ± 0.74 μM; mean ± SD, n = 3; **Fig. 6E**).

In order to substantiate the molecular changes underlying antiproliferative effects of AQ we examined modulation of protein regulators determining G_1/S transition focusing on those that displayed major AQ-induced expression changes as detected by array analysis including TP53, CDKN1A, and E2F1 (**Fig. 6A and B**). We also examined CCND1 (cyclin D1), phosphorylation status of RB1 (retinoblastoma 1), and MYC. Immunoblot analysis revealed pronounced upregulation of CDKN1A protein levels, a potent cyclin-dependent kinase inhibitor that directly inhibits the activity of CCNE (cyclin E)-CDK2 and CCND-CDK4/6 complexes involved in G_1/S phase transition and progression.[60,66] Consistent with the observed dose-dependent upregulation of *CDKN1A* mRNA and CDKN1A protein levels (**Fig. 5**; **Fig. 6A and C**), upregulation of TP53, the transcriptional regulator of *CDKN1A*, was observed at the transcriptional (*TP53* [**Fig. 5B**]) and protein levels (**Fig. 6A**). Moreover, moderate suppression of CCND1 protein levels occurred in response to AQ treatment (**Fig. 6A**).

Next, we focused on *E2F1*, the gene that displayed the most pronounced downregulation at the transcriptional level (**Fig. 5A and B**). Remarkably, AQ-suppression of *E2F1* expression was confirmed at the protein level (**Fig. 6A**). E2F1 is a transcription factor and master regulator of cell proliferation, expressed mainly at late G_1 and G_1/S transition in all actively proliferating tissues.[67-69] We also examined AQ modulation of RB1, the upstream regulator of E2F1 function. AQ treatment caused pronounced reactivation of RB1 tumor suppressor function by removal of inhibitory phosphorylations at Ser780 and Ser807/811 that interfere with E2F1 sequestration, established sites of posttranslational RB1 regulation at the G_1/S checkpoint.[70,71] Since AQ modulated a number of major cell cycle regulators (TP53, CDKN1A, CCND1, E2F1, RB1) that are involved in functional crosstalk with MYC we also examined expression of this master regulator of cell proliferation. However, only moderate downregulation at the protein level was observed (**Fig. 6A**). Importantly, key expression changes induced by AQ in A375 malignant melanoma cells were also observed in metastatic melanoma cells including G361 cells, where immunoblot detection confirmed downregulation of heat shock proteins (HSPA1A, HSP90AA1) and pronounced upregulation of CDKN1A, consistent with the antiproliferative activity of AQ (**Fig. 6B**).

In the context of our expression array-guided exploration of AQ-induced antimelanoma effects, it should be mentioned that immunoblot detection did not always confirm changes observed at the mRNA level. For example, significant downregulation of *RPL13A* mRNA (- 3.5 fold; encoding 60S ribosomal protein L13a; **Fig. 5A and B**) was detected by expression array analysis but could not be substantiated at the protein level (RPL13A; **Fig. 6A**). Therefore, other significant AQ-induced changes observed at the mRNA level as summarized in **Figure 5B** await further validation and functional exploration.

Inhibitory activity of AQ on lysosomal function and proliferation of melanoma cells surpasses that of CQ

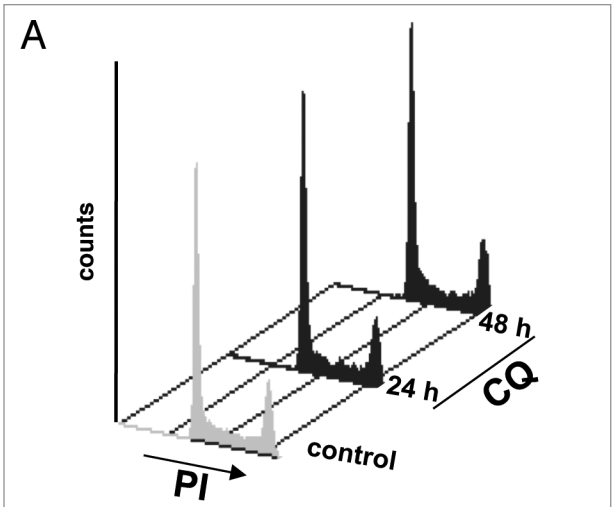

B

	distribution [% total]		
	G_1	S	G_2/M
control	51.8±2.6	32.0±6.9	16.2± 5.7
CQ (10μM, 24hr)	49.7±1.7	35.0±1.1	15.4±2.7
CQ (10μM, 48hr)	51.5±11.4	31.1±6.3	17.4±5.2

Figure 8. Analysis of CQ-induced alterations of cell cycle distribution. (**A**) Representative histogram depicting cell cycle distribution after treatment with CQ (10 μM, ≤ 48 h). After treatment for the indicated time periods, cells were stained with PI and analyzed by flow cytometry. (**B**) The data indicate the percentage of cells in each phase of the cell cycle; the table summarizes results from 3 independent repeat experiments (mean ± SD [n = 3]).

After investigating the antimelanoma activity of AQ, we compared chemotherapeutic efficacy between the 4-aminoquinoline antimalarials AQ and its parent compound CQ (**Fig. 6E**; **Fig. 7**). First, we compared the potency of anti-proliferative activity displayed by CQ vs. AQ (**Fig. 6E**). A comparative dose response relationship analysis performed in A375 (AQ: IC_{50} = 0.32 ± 0.12 μM; CQ: IC_{50} = 2.81 ± 0.44 μM), G361 (AQ: IC_{50} = 0.71 ± 0.16 μM; CQ: IC_{50} = 12.63 ± 2.55 μM), and LOX (AQ: IC_{50} = 2.60 ± 0.74; CQ: IC_{50} = 8.38 ± 0.93 μM; mean ± SD, n = 3) melanoma cells identified AQ as the superior inhibitor of melanoma cell proliferation among the 2 tested 4-aminoquinoline antimalarials.

Next, we examined the induction of autophagic-lysosomal impairment in CQ-treated A375 melanoma cells. We observed that CQ-induced morphological changes examined by transmission electron microscopy were similar to those induced by AQ, including formation of multivesicular, single membrane-enclosed structures containing electron-dense osmiophilic inclusions (**Fig. 7A**). However, morphological changes elicited by CQ seemed less pronounced (number and size of multivesicular structures) compared with those induced by AQ exposure (**Fig. 1C and D** vs. **Fig. 7A**). Further analysis revealed CQ-induced effects on autophagic-lysosomal function similar to those observed with AQ monitoring RFP-GFP-LC3 puncta formation (**Fig. 7B**). As observed earlier with AQ (**Fig. 2D**), exposure to CQ caused formation of LC3 puncta that displayed both green and red fluorescence producing a yellow overlay, a finding consistent with the established ability of the lysosomotropic agent CQ to induce autophagic-lysosomal blockade through impairment of lysosomal pH-control and function thereby inducing accumulation of dysfunctional autolysosomes with colocalization of GFP- and RRP-labeled LC3. Immunoblot analysis demonstrated CQ-induced accumulation of LAMP1, LC3-II, and SQSTM1 (**Fig. 7G**), changes similar to AQ-induced alterations (**Fig. 2A and C**). Moreover, consistent with prior reports, CQ treatment caused a significant inhibition of lysosomal cathepsin activity (CTSB, CTSL, CTSD; **Fig. 7C and D**).[72] Importantly, when cathepsin-directed inhibitory effects were compared between CQ and AQ (10 μM, each), it was observed that AQ caused a more pronounced reduction of CTSL and CTSD enzymatic activity, whereas CQ and AQ were equally effective antagonizing CTSB enzymatic activity (**Fig. 7D**). Differential suppression of lysosomal cathepsin activity by AQ vs. CQ correlates well with the occurrence of more pronounced morphological changes at the lysosomal level observed in AQ-exposed melanoma cells (**Fig. 1C and D** vs. **Fig. 7A**).

After identifying AQ as the superior inhibitor of melanoma cell proliferation among the two tested 4-aminoquinoline antimalarials (**Fig. 6E**), we also performed comparative gene expression analysis indicating that CQ-induced changes at the mRNA level did not match those detected in response to AQ (**Fig. 7E**). Specifically, CQ treatment failed to change expression of AQ-responsive key genes including *DDIT3*, *CDKN1A*, *GADD45A*, *EGR1*, and *E2F1*. Consistent with the inferior anti-proliferative potency of CQ as compared with AQ, subsequent immunoblot analysis demonstrated that even though CQ treatment caused moderate upregulation of CDKN1A protein levels, CQ failed to alter protein levels of TP53, E2F1, CCND1, and HSPA1A, changes observed earlier in response to AQ treatment (**Fig. 7F and G**). Indeed, further analysis indicated that CQ treatment was not associated with the induction of cell cycle arrest (**Fig. 8**), an observation strikingly different from AQ-induced melanoma cell cycle blockade in S phase (**Fig. 6D**).

Discussion

Pharmacological inhibition of autophagic-lysosomal function has recently emerged as a promising strategy for chemotherapeutic intervention targeting cancer cells.[4,5,9,13-15] Even though numerous ongoing clinical trials aim at substantiating favorable therapeutic effects of chloroquine and hydroxychloroquine, the limited therapeutic performance of these lysosomotropic 4-aminoquinoline derivatives prompted us to explore other promising drug candidates that target autophagic-lysosomal function in cancer cells.

In this study we have examined the antimelanoma activity of the antimalarial AQ and have observed that in cultured malignant melanoma cells AQ causes pronounced autophagic-lysosomal and proliferative blockade that surpasses that of its parent compound CQ. AQ-induced autophagic-lysosomal antagonism was associated with early inhibition of cathepsin enzymatic activity (CTSB, CTSL, CTSD; **Fig. 3B and C**) and ATP depletion,

both detectable within 1 h exposure time (**Fig. 4B**). AQ-imposed impairment of autophagic-lysosomal function was further substantiated by ultrastructural changes observed by electron microscopy (**Fig. 1**), GFP-RFP-LC3 fluorescence imaging (**Fig. 2D**), and immunoblot detection of specific protein markers (LAMP1, LC3-II) and autophagy substrates (SQSTM1, SNCA; **Fig. 2A and C**).

Concerning the mechanism of AQ-induced autophagic-lysosomal alterations observed in human melanoma cells, our data are most consistent with a functional blockade imposed by AQ at the lysosomal level.[49,73] Aminoquinoline-antimalarials (including CQ and AQ) are established lysosomotropic agents that cause lysosomal disruption with impairment of pH control and inactivation of lysosomal proteases (including cathepsins), a mechanism of action underlying antimalarial activity through disruption of the acidic food vacuole of the parasite.[51] We observed that lysosomal cathepsin activity was impaired rapidly (**Fig. 3B and C**), and a similar pattern of puncta formation was imposed by the lysosomally-targeted agent BafA or AQ as evidenced by RFP-GFP-LC3 fluorescence (**Fig. 2D**). Moreover, the LC3 turnover assay employing BafA did not indicate an upregulation of autophagic flux in response to AQ (**Fig. 3A**), and no accumulation of double-membrane structures that would be indicative of increased autophagosome formation was observed by electron microscopy. In contrast, we only detected accumulation of large single membrane-enclosed, multivesicular structures displaying pronounced osmiophilicity, consistent with autolysosomal aggregation and accumulation of undigested cargo and lipofuscin in response to AQ.

In addition to the causation of autophagic-lysosomal alterations, we also observed that AQ treatment blocked melanoma cell cycle progression in S-phase (**Fig. 6D**). It is important to note that induction of mitotic arrest in response to lysosomotropic agents has been observed before and was attributed to impaired macroautophagy and TP53-mediated effects,[51,74] molecular changes that also occur in response to AQ treatment (**Figs. 1, 2, and 6**). Our own array analysis revealed modulation of gene expression antagonizing cell cycle progression (*CDKN1A* upregulation, *E2F1* downregulation), and immunoblot detection demonstrated AQ-modulation of TP53, CDKN1A, E2F1, CCND1, and phosphorylated RB1 (Ser780 and 807/811). Indeed, AQ displayed potent antiproliferative effects causing S-phase arrest at submicromolar concentrations (**Fig. 6D and E**). Downregulation of *E2F1* expression, the gene displaying the highest AQ-induced expression differential at the mRNA level (**Fig. 5**), is of particular interest since pharmacological E2F1 antagonism has recently emerged as a promising antiproliferative strategy targeting melanoma.[67] Indeed, we observed AQ-induced downregulation of E2F1 protein levels at concentrations as low as 1 μM (**Fig. 6A**). However, the specific mechanisms and upstream events underlying AQ-induced proliferative blockade as shown here for the first time in human melanoma cells remain to be elucidated. In the context of AQ-induced cell cycle arrest that occurs in S-phase rather than in G_1-phase, it should be mentioned that earlier research has demonstrated that overexpression or pharmacological upregulation of *CDKN1A* expression, the cell cycle regulator displaying the most pronounced expression changes in response to AQ treatment at both the mRNA and protein levels (**Fig. 5B**; **Fig. 6A and C**), may indeed cause S-phase arrest,[60,75,76] and pharmacological downregulation of CCND1 as well as dephosphorylation of RB1, as observed by us in response to AQ treatment, have also been documented in association with S-phase arrest.[77,78]

Our experiments document for the first time that AQ treatment causes the rapid induction of energy crisis (**Fig. 4B**), impairment of mitochondrial transmembrane potential (**Fig. 4C**), and the blockade of starvation-induced autophagic-lysosomal adaptations in malignant melanoma cells (**Fig. 4A**). This activity may sensitize melanoma cells to the cytotoxic metabolic stress imposed by prolonged starvation, a hypothesis substantiated by our observation that the combined exposure to AQ and starvation by culture in HBSS causes massive melanoma cell death (**Fig. 4D**). Likewise, the observation that AQ causes chemosensitization to standard chemotherapeutic agents (CDDP, Doxo; **Fig. 4E and F**) suggests that combination therapy employing chemotherapeutics together with this clinical antimalarial may provide improved therapeutic efficacy, a hypothesis to be tested in the future. However, the specific mechanism underlying AQ-dependent chemosensitization and increased vulnerability to starvation-induced cell death remains undefined and may involve causative factors beyond autophagic-lysosomal modulation such as impairment of mitochondrial transmembrane potential,[58,79] known to occur in response to treatment with other 4-aminoquinoline antimalarials and observed here for the first time with AQ.[51,56] Interestingly, it has recently been observed that CQ sensitizes breast cancer cells to chemotherapy independent of autophagy, and similar mechanisms may apply to AQ-induced sensitization.[80] Moreover, massive downregulation of heat shock response gene expression as observed by us at the mRNA (e.g., *HSPA8*, *HSPA1A*, *HSP90AA1*; **Fig. 5**; **Fig. 6C**) and protein level (HSPA1A, HSP90AA1; **Fig. 6A and B**) may also contribute to AQ-induced sensitization to cytotoxic stress, a hypothesis consistent with the established cytoprotective and antiapoptotic role of these heat shock proteins in melanoma and other cancer cells.[61,81,82]

Currently, the molecular basis underlying the more potent antimelanoma activity of AQ vs. CQ remains undefined. It is noteworthy that AQ also displays more potent antimalaria activity, a property attributed before to its increased tropism targeting the acidic food vacuole of the plasmodium parasite,[83-86] but additional structural features may contribute to increased potency of the drug. As with its parent compound CQ, AQ is a lysosomotropic 4-aminoquinoline-based tertiary amine, but only AQ contains a 1,4-aminophenol-substituent that forms an electrophilic quinoneimine-metabolite upon intracellular oxidation, a reactive intermediate that may be involved in covalent protein adduction.[47,48] Indeed, other drugs containing aminophenol-pharmacophores cause inhibitory adduction at cysteine-residues of specific target proteins such as CTSB.[87] It is therefore tempting to speculate that in addition to disruption of lysosomal pH control, a physicochemical effect commonly associated with the class of 4-aminoquinoline antimalarials, covalent adduction of specific protein targets by AQ my contribute to its higher

antimelanoma activity, a hypothesis to be tested by future experiments. Consistent with this hypothesis, using a monoclonal antibody employed clinically for ELISA-detection of AQ-adducted plasma protein, we detected the accumulation of AQ-modified proteins (35- to 55-kDa molecular mass range) in melanoma cells (**Fig. 2A**). Currently, we are employing proteomic tools in order to elucidate identity and functional implications of specific AQ-adducted target proteins in melanoma cells.

The concept of repurposing clinical antimalarials (including CQ, hydroxychloroquine, primaquine, and artemisinin-derivatives) for cancer chemotherapy has recently gained considerable attention.[4,14,18-20,22,23,33,34] AQ is in clinical use worldwide (yet not in the United States) as an antimalarial equivalent to CQ, and recent studies have shown that AQ is superior to CQ in the treatment of resistant strains of *Plasmodium falcip*arum.[83] Remarkably, safety and efficacy of AQ-based antimalarial therapy are well established, and pharmacogenetic profiling of an AQ-metabolizing enzyme (cytochrome P450, family 2, subfamily C, polypeptide 8; encoded by *CYP2C8*) in malaria patients may improve the safe use of this drug.[88,89] Taken together, our data suggest that AQ is a promising candidate for drug repurposing efforts aimed at undermining autophagic-lysosomal function and proliferative control in malignant melanoma cells. Our current research efforts aim at the identification of specific molecular targets involved in AQ-based inactivation of cancer cells, and studies that aim at demonstrating feasibility of AQ-based adjuvant chemotherapeutic intervention in preclinical murine models of human melanoma have been initiated.

Materials and Methods

Chemicals

All chemicals were purchased from Sigma Chemical Co. (bafilomycin A1, B1793; chloroquine, C6628; cis-dichlorodiamine-platinum [II], P4394; doxorubicin, D1515) except amodiaquine (Fluka, A2799).

Cell culture

Human malignant A375 melanoma cells (ATCC, CRL-1619) were cultured in RPMI medium (ATCC, 30-2001) containing 10% bovine calf serum (Hyclone, SH30072.03). LOX-IMVI human metastatic melanoma cells (a gift from G. Paine-Murrieta, University of Arizona) were cultured exactly as A375 cells, and G361 (ATCC, CRL-1424) human metastatic melanoma cells were cultured in McCoy's 5a medium (ATCC, 30-2007) containing 10% bovine calf serum. Cells were maintained at 37 °C in 5% CO_2, 95% air in a humidified incubator. Dulbecco's phosphate-buffered saline (PBS) and HBSS containing 5.6 mM D-glucose were from Life Technologies (14199-144 and 14025-092).

Transmission electron microscopy

Cells were fixed in situ with 2.5% glutaraldehyde in 0.1 M cacodylate buffer (pH 7.4), post-fixed in 1% osmium tetroxide in cacodylate buffer, washed, scraped and pelleted as described recently.[7,33] Cells were then stained in 2% aqueous uranyl acetate, dehydrated through a graded series (50, 70, 90, and 100%) of ethanol and infiltrated with Spurr's resin (Sigma, EM0300), then allowed to polymerize overnight at 60 °C. Sections (50 nm) were cut, mounted onto uncoated 150-mesh copper grids, and stained with 2% lead citrate. Sections were examined in a CM12 transmission electron microscope (FEI) operated at 80 kV with digital image collection.

Flow cytometric quantification of cellular autofluorescence

After AQ treatment, cells were harvested, washed and resuspended in 300 μl PBS, and immediately analyzed by flow cytometry (λ_{ex} 488 nm, λ_{em} 585 ± 42 nm) as published recently.[38]

RFP-GFP-LC3 puncta formation assay

A375 cells were grown on 35-mm glass bottom dishes (MatTek, P35G-0-10-C) for live-cell imaging. Cells were transfected with an mRFP-EGFP-LC3 construct (Addgene, 21074:ptfLC3) following a published procedure.[6] Twenty-four hours after transfection followed by AQ treatment (10 μM, up to 24 h), cells were gently washed once with PBS, and phenol red-free DMEM supplemented with 10% FBS was added. All images were taken with the Zeiss Observer Z1 microscope using the Slidebook 4.2.0.11 computer program (Intelligent Imaging Innovations, Inc.).

Cell proliferation assay

Cells were seeded at 5,000 cells/dish on 35-mm dishes. After 24 h, cells were exposed to a test compound (CQ vs. AQ, 0.1–10 μM; 72 h continuous exposure). Numbers of adherent cells at the time of compound addition and 72 h later were determined using a Z2 analyzer (Beckman Coulter, Inc.). Proliferation was compared with cells that received mock treatment. The same methodology was used to establish IC_{50} values (drug concentration that induces 50% inhibition of proliferation) indicating antiproliferative potency.

Flow cytometric analysis of cell viability

Viability and induction of cell death (early and late apoptosis/necrosis) were examined by ANXA5/annexin AV-FITC/propidium iodide (PI) dual staining of cells followed by flow cytometric analysis as published previously.[33,64] Cells (100,000) were seeded on 35-mm dishes and received drug treatment 24 h later. Cells were harvested at various time points after treatment and cell staining was performed using an apoptosis detection kit according to the manufacturer's specifications (Sigma, APOAF-20TST). Viable cells are located in the bottom left quadrant ($ANXA5^-$, PI^-), whereas early apoptotic and late apoptotic/necrotic cells are located in the bottom right ($ANXA5^+$, PI^-) and top right quadrant ($ANXA5^+$, PI^+), respectively.

Cell cycle analysis

Cells were seeded at 25,000 per 35-mm dish and left overnight to attach. The next day, cells received treatment with test compounds and vehicle controls. After 24 and 48 h continuous drug exposure, cells were processed as published before.[65] Cellular DNA content was determined by flow cytometry and analyzed using the ModFitLT software, version 4.0 (Verity, VMFLTMAC4).

Cellular ATP determination

Cells were seeded at 50,000 cells/dish on 35-mm dishes. After 24 h, cells were treated with test compound (AQ ≤ 10 μM). At various time points (≤ 24 h) cells were counted, and ATP content per 5,000 cells was determined using the CellTiter-Glo luminescent assay (Promega, G7571) according to the manufacturer's

instructions as published earlier.[59,65,90] Data are normalized to ATP content in untreated cells.

Mitochondrial transmembrane potential

Mitochondrial transmembrane potential ($\Delta\psi m$) was assessed using the potentiometric dye 5,5′,6,6′-tetrachloro-1,1′,3,3′-tetraethylbenzimidazolyl-carbocyanine iodide (JC-1; Sigma, T4069) following our published procedure.[33,64] In brief, cells were trypsinized, washed in PBS, resuspended in 300 μl PBS containing 5 μg/ml JC-1 for 15 min at 37 °C and 5% CO_2 in the dark, then washed twice in PBS and resuspended in 300 μl PBS. Bivariate analysis was performed by flow cytometry with excitation at 488 nm, and mitochondrial function was assessed as JC-1 green (depolarized mitochondria, detector FL-1) or red (polarized mitochondria, detector FL-2) fluorescence.

Enzymatic activity of CTSB, L, and D

CTSB activity was measured using a fluorimetric CTSB activity assay kit (BioVision, K140-100), according to the manufacturer's instructions as published recently.[8,38] Cells (1×10^6) were lysed in 0.5 ml of chilled lysis buffer. After 10 min incubation on ice, lysates were centrifuged at 10,000 g at 4 °C for 5 min and the supernatant fraction was retained for analysis. 50 μl of cell lysate was incubated with 50 μl of reaction buffer. CTSB substrate (Ac-RR-AFC; 200 μM final concentration) was then added and the mixture was incubated for 1 h at 37 °C. As a negative control, analysis was performed in the presence of the CTSB/L inhibitor Z-Phe-Phe-FMK (Sigma, C9109; 20 μM final concentration). The release of free amino-4-trifluoromethylcoumarin (AFC) was measured using a fluorescence plate reader (λ*ex* 400 nm; λ*em* 505 nm; SpectraMax Gemini, Molecular Devices). Protein concentration of cell lysates was determined using a BCA protein assay kit (Pierce, 23227), and cathepsin activity was normalized to protein concentrations.

CTSD and CTSL activities were determined using fluorimetric assay kits (BioVision, K143-100 and K142-100) according to the manufacturer's instructions as published recently.[8] Processing of samples and the protocol were identical to the CTSB activity assay as described above with the following modifications: CTSL determination: After lysis, 50 μL lysate were incubated with 50 μL of reaction buffer containing Ca074 (Sigma, C5732; 1 μM, 15 min) to irreversibly inhibit CTSB, thereby eliminating interference from CTSB-dependent cleavage of the substrate.[91,92] CTSL substrate (Ac-Phe-Arg-AFC, Abcam, ab157769; 200 μM final concentration) was then added and the mixture was incubated for 1 h at 37 °C followed by AFC detection (λ*ex* 400 nm, λ*em* 505 nm). As a negative control, analysis was performed in the presence of Z-Phe-Phe-FMK (200 μM final concentration). CTSD determination: Using CTSD substrate (MCA-GKPILFFRLK[Dnp]-DR-NH2, Abcam, ab126779; 200 μM final concentration) the release of free 7-methoxycoumarin-4-yl acetyl was measured using a fluorescence plate reader (λ*ex* 328 nm; λ*em* 460 nm).

Human Stress and Toxicity RT²Profiler™ PCR expression array analysis

After pharmacological exposure, total cellular RNA (3×10^6 A375 cells) was prepared according to a standard procedure using the RNeasy kit (Qiagen, 74104). Reverse transcription was performed using the RT² First Strand kit (Superarray, 330401) and 5 μg total RNA as described previously.[33,62] The Human Autophagy RT²Profiler™ PCR Expression Array (Qiagen, PAHS-084ZA-12) and the Human Stress and Toxicity RT²Profiler™ PCR Expression Array (Qiagen, PAHS-003A-12), each profiling the expression of 84 genes, was run using the following PCR conditions: 95 °C for 10 min, followed by 40 cycles of 95 °C for 15 s alternating with 60 °C for 1 min (Applied Biosystems, 7000 SDS). Gene-specific product was normalized to *GAPDH* and quantified using the comparative ($\Delta\Delta C_t$) Ct method as described in the ABI Prism 7000 sequence detection system user guide as published earlier.[33,62] Expression values were averaged across 3 independent array experiments, and standard deviation was calculated for graphing.

Gene expression analysis by real time RT-PCR

After AQ exposure (1–20 μM, 24 h), total cellular RNA (3×10^6 cells) was prepared using the RNEasy kit (Qiagen, 74104). Reverse transcription was performed using TagMan Reverse Transcription Reagents and 200 ng of total RNA in a 50-μl reaction. Reverse transcription was primed with random hexamers and incubated at 25 °C for 10 min followed by 48 °C for 30 min, 95 °C for 5 min, and a chill at 4 °C. Each PCR reaction consisted of 3.75 μl of cDNA added to 12.5 μl of TaqMan Universal PCR Master Mix (Roche Molecular Systems), 1.25 μl of gene specific primer/probe mix (Assay-by-Design; Applied Biosystems: *CDKN1A* [assay ID Hs00355782_m1], *DDIT3* [assay ID Hs00358796_g1], *GADD45A* [assay ID Hs00169255_m1], *HSPA1A* [assay ID Hs00359163_s1], *EGR1* [assay ID Hs00152928_m1], *E2F1* [assay ID Hs00153451_m1], and *GAPDH* [assay ID Hs99999905_m1]) and 7.5 μl of PCR water. PCR conditions were: 95 °C for 10 min, followed by 40 cycles of 95 °C for 15 s alternating with 60 °C for 1 min (Applied Biosystems 7000 SDS). Gene-specific product was normalized to GAPDH and quantified using the comparative ($\Delta\Delta C_t$) Ct method as described in the ABI Prism 7000 sequence detection system user guide as published earlier.[33,62]

Immunoblot detection

Cells were lysed in 1× SDS-PAGE sample buffer and heated for 3 min at 95 °C. Samples were separated by 12% SDS-PAGE followed by transfer to Protran nitrocellulose membranes (Whatman, BA85). Membranes were incubated with primary antibodies in 5% milk-TBST overnight at 4 °C as follows: rabbit anti-phospho-RB1(Ser780) polyclonal (Cell Signaling Technology, 9307); rabbit anti-phospho-RB1(Ser807/811) polyclonal (Cell Signaling Technology, 9308); mouse anti-RB1 monoclonal (Cell Signaling Technology, 9309); mouse anti-CDKN1A monoclonal (Cell Signaling Technology, 2946); rabbit anti-LAMP1 monoclonal (Cell Signaling Technology, 3243); rabbit anti-SNCA polyclonal (Cell Signaling Technology, 4179); rabbit anti-RPL13A polyclonal (Cell Signaling Technology, 2765); rabbit anti-MYC monoclonal (Cell Signaling Technology, 5605P); mouse anti-TP53 monoclonal (Santa Cruz Biotechnology, sc-126); mouse anti-E2F1 monoclonal (Santa Cruz Biotechnology, sc-251); mouse anti-BECN1 monoclonal (Santa Cruz Biotechnology, sc-48341); anti-CCND1 polyclonal (Santa Cruz Biotechnology, sc-718); mouse anti-SQSTM1/p62 monoclonal (Santa Cruz

Biotechnology, sc-48402); rabbit anti-LC3 polyclonal (Novus Biologics, 100-2331); mouse anti-HSPA1A/Hsp70 monoclonal (Enzo Life Sciences, SPA-810-F); anti-HSP90AA1/Hsp90 monoclonal (Enzo Life Sciences, SPA-836-D); mouse anti-amodiaquine monoclonal (Thermo Scientific, 320-04-02). Use of HRP-conjugated goat anti-rabbit (Jackson Immunological Research, 111-035-144) or goat anti-mouse secondary antibody (Jackson Immunological Research, 115-035-146) was followed by visualization using enhanced chemiluminescence detection reagents. Equal protein loading was examined using a mouse anti-ACTB monoclonal antibody (Sigma, A4700).

Statistical analysis

The results are presented as means (± S.D.) of at least three independent experiments. Data were analyzed employing the two-sided Student *t* test; differences were considered significant at $P < 0.05$ ($^{*}P < 0.05$; $^{**}P < 0.01$; $^{***}P < 0.001$). Selected data sets were analyzed employing one-way analysis of variance (ANOVA) with Tukey's post hoc test using the PRISM 4.0 software; means without a common letter differ from each other ($P < 0.05$).

Disclosure of Potential Conflicts of Interest

The authors have no conflicts of interest to declare. There are no financial disclosures to be made.

Acknowledgments

Supported in part by grants from the National Institutes of Health (R01CA122484, R03CA167580, R21CA166926, ES007091, ES06694, Arizona Cancer Center Support Grant CA023074). The content is solely the responsibility of the authors and does not necessarily represent the official views of the National Cancer Institute or the National Institutes of Health.

References

1. Klionsky DJ. Autophagy: from phenomenology to molecular understanding in less than a decade. Nat Rev Mol Cell Biol 2007; 8:931-7; PMID:17712358; http://dx.doi.org/10.1038/nrm2245
2. Mizushima N, Levine B, Cuervo AM, Klionsky DJ. Autophagy fights disease through cellular self-digestion. Nature 2008; 451:1069-75; PMID:18305538; http://dx.doi.org/10.1038/nature06639
3. Cecconi F, Levine B. The role of autophagy in mammalian development: cell makeover rather than cell death. Dev Cell 2008; 15:344-57; PMID:18804433; http://dx.doi.org/10.1016/j.devcel.2008.08.012
4. Rubinsztein DC, Codogno P, Levine B. Autophagy modulation as a potential therapeutic target for diverse diseases. Nat Rev Drug Discov 2012; 11:709-30; PMID:22935804; http://dx.doi.org/10.1038/nrd3802
5. Benbrook DM, Long A. Integration of autophagy, proteasomal degradation, unfolded protein response and apoptosis. Exp Oncol 2012; 34:286-97; PMID:23070014
6. Lau A, Zheng Y, Tao S, Wang H, Whitman SA, White E, Zhang DD. Arsenic inhibits autophagic flux, activating the Nrf2-Keap1 pathway in a p62-dependent manner. Mol Cell Biol 2013; 33:2436-46; PMID:23589329; http://dx.doi.org/10.1128/MCB.01748-12
7. Lamore SD, Wondrak GT. Autophagic-lysosomal dysregulation downstream of cathepsin B inactivation in human skin fibroblasts exposed to UVA. Photochem Photobiol Sci 2012; 11:163-72; PMID:21773629; http://dx.doi.org/10.1039/c1pp05131h
8. Lamore SD, Wondrak GT. UVA causes dual inactivation of cathepsin B and L underlying lysosomal dysfunction in human dermal fibroblasts. J Photochem Photobiol B 2013; 123:1-12; PMID:23603447; http://dx.doi.org/10.1016/j.jphotobiol.2013.03.007
9. Amaravadi RK, Lippincott-Schwartz J, Yin XM, Weiss WA, Takebe N, Timmer W, DiPaola RS, Lotze MT, White E. Principles and current strategies for targeting autophagy for cancer treatment. Clin Cancer Res 2011; 17:654-66; PMID:21325294; http://dx.doi.org/10.1158/1078-0432.CCR-10-2634
10. Sheen JH, Zoncu R, Kim D, Sabatini DM. Defective regulation of autophagy upon leucine deprivation reveals a targetable liability of human melanoma cells in vitro and in vivo. Cancer Cell 2011; 19:613-28; PMID:21575862; http://dx.doi.org/10.1016/j.ccr.2011.03.012
11. Yu H, Su J, Xu Y, Kang J, Li H, Zhang L, Yi H, Xiang X, Liu F, Sun L. p62/SQSTM1 involved in cisplatin resistance in human ovarian cancer cells by clearing ubiquitinated proteins. Eur J Cancer 2011; 47:1585-94; PMID:21371883; http://dx.doi.org/10.1016/j.ejca.2011.01.019
12. O'Donovan TR, O'Sullivan GC, McKenna SL. Induction of autophagy by drug-resistant esophageal cancer cells promotes their survival and recovery following treatment with chemotherapeutics. Autophagy 2011; 7:509-24; PMID:21325880; http://dx.doi.org/10.4161/auto.7.5.15066
13. Amaravadi RK, Yu D, Lum JJ, Bui T, Christophorou MA, Evan GI, Thomas-Tikhonenko A, Thompson CB. Autophagy inhibition enhances therapy-induced apoptosis in a Myc-induced model of lymphoma. J Clin Invest 2007; 117:326-36; PMID:17235397; http://dx.doi.org/10.1172/JCI28833
14. Degtyarev M, De Mazière A, Klumperman J, Lin K. Autophagy, an Achilles' heel AKTing against cancer? Autophagy 2009; 5:415-8; PMID:19305139; http://dx.doi.org/10.4161/auto.5.3.7827
15. Xie X, White EP, Mehnert JM. Coordinate autophagy and mTOR pathway inhibition enhances cell death in melanoma. PLoS One 2013; 8:e55096; PMID:23383069; http://dx.doi.org/10.1371/journal.pone.0055096
16. Reaume AG. Drug repurposing through nonhypothesis driven phenotypic screening. Drug Discov Today 2011; 8:85-8
17. Weir SJ, DeGennaro LJ, Austin CP. Repurposing approved and abandoned drugs for the treatment and prevention of cancer through public-private partnership. Cancer Res 2012; 72:1055-8; PMID:22246671; http://dx.doi.org/10.1158/0008-5472.CAN-11-3439
18. Neznanov N, Gorbachev AV, Neznanova L, Komarov AP, Gurova KV, Gasparian AV, Banerjee AK, Almasan A, Fairchild RL, Gudkov AV. Antimalaria drug blocks proteotoxic stress response: anti-cancer implications. Cell Cycle 2009; 8:3960-70; PMID:19901558; http://dx.doi.org/10.4161/cc.8.23.10179
19. Garber K. Inducing indigestion: companies embrace autophagy inhibitors. J Natl Cancer Inst 2011; 103:708-10; PMID:21515831; http://dx.doi.org/10.1093/jnci/djr168
20. Sharma N, Thomas S, Golden EB, Hofman FM, Chen TC, Petasis NA, Schönthal AH, Louie SG. Inhibition of autophagy and induction of breast cancer cell death by mefloquine, an antimalarial agent. Cancer Lett 2012; 326:143-54; PMID:22863539; http://dx.doi.org/10.1016/j.canlet.2012.07.029
21. Solomon VR, Lee H. Chloroquine and its analogs: a new promise of an old drug for effective and safe cancer therapies. Eur J Pharmacol 2009; 625:220-33; PMID:19836374; http://dx.doi.org/10.1016/j.ejphar.2009.06.063
22. Sukhai MA, Prabha S, Hurren R, Rutledge AC, Lee AY, Sriskanthadevan S, Sun H, Wang X, Skrtic M, Seneviratne A, et al. Lysosomal disruption preferentially targets acute myeloid leukemia cells and progenitors. J Clin Invest 2013; 123:315-28; PMID:23202731; http://dx.doi.org/10.1172/JCI64180
23. Bristol ML, Emery SM, Maycotte P, Thorburn A, Chakradeo S, Gewirtz DA. Autophagy inhibition for chemosensitization and radiosensitization in cancer: do the preclinical data support this therapeutic strategy? J Pharmacol Exp Ther 2013; 344:544-52; PMID:23291713; http://dx.doi.org/10.1124/jpet.112.199802
24. Kimura T, Takabatake Y, Takahashi A, Isaka Y. Chloroquine in cancer therapy: a double-edged sword of autophagy. Cancer Res 2013; 73:3-7; PMID:23288916; http://dx.doi.org/10.1158/0008-5472.CAN-12-2464
25. Garbe C, Eigentler TK, Keilholz U, Hauschild A, Kirkwood JM. Systematic review of medical treatment in melanoma: current status and future prospects. Oncologist 2011; 16:5-24; PMID:21212434; http://dx.doi.org/10.1634/theoncologist.2010-0190
26. Ibrahim N, Haluska FG. Molecular pathogenesis of cutaneous melanocytic neoplasms. Annu Rev Pathol 2009; 4:551-79; PMID:19400696; http://dx.doi.org/10.1146/annurev.pathol.3.121806.151541
27. Aplin AE, Kaplan FM, Shao Y. Mechanisms of resistance to RAF inhibitors in melanoma. J Invest Dermatol 2011; 131:1817-20; PMID:21593776; http://dx.doi.org/10.1038/jid.2011.147
28. Armstrong JL, Corazzari M, Martin S, Pagliarini V, Falasca L, Hill DS, Ellis N, Al Sabah S, Redfern CP, Fimia GM, et al. Oncogenic B-RAF signaling in melanoma impairs the therapeutic advantage of autophagy inhibition. Clin Cancer Res 2011; 17:2216-26; PMID:21270111; http://dx.doi.org/10.1158/1078-0432.CCR-10-3003
29. Marino ML, Pellegrini P, Di Lernia G, Djavaheri-Mergny M, Brnjic S, Zhang X, Hägg M, Linder S, Fais S, Codogno P, et al. Autophagy is a protective mechanism for human melanoma cells under acidic stress. J Biol Chem 2012; 287:30664-76; PMID:22761435; http://dx.doi.org/10.1074/jbc.M112.339127

30. Ma XH, Piao S, Wang D, McAfee QW, Nathanson KL, Lum JJ, Li LZ, Amaravadi RK. Measurements of tumor cell autophagy predict invasiveness, resistance to chemotherapy, and survival in melanoma. Clin Cancer Res 2011; 17:3478-89; PMID:21325076; http://dx.doi.org/10.1158/1078-0432.CCR-10-2372
31. Flemming A. Cancer: Autophagy presents Achilles heel in melanoma. Nat Rev Drug Discov 2011; 10:491; PMID:21720400; http://dx.doi.org/10.1038/nrd3482
32. Del Bello B, Toscano M, Moretti D, Maellaro E. Cisplatin-induced apoptosis inhibits autophagy, which acts as a pro-survival mechanism in human melanoma cells. PLoS One 2013; 8:e57236; PMID:23437349; http://dx.doi.org/10.1371/journal.pone.0057236
33. Cabello CM, Lamore SD, Bair WB 3rd, Qiao S, Azimian S, Lesson JL, Wondrak GT. The redox antimalarial dihydroartemisinin targets human metastatic melanoma cells but not primary melanocytes with induction of NOXA-dependent apoptosis. Invest New Drugs 2012; 30:1289-301; PMID:21547369; http://dx.doi.org/10.1007/s10637-011-9676-7
34. Wondrak GT. Redox-directed cancer therapeutics: molecular mechanisms and opportunities. Antioxid Redox Signal 2009; 11:3013-69; PMID:19496700; http://dx.doi.org/10.1089/ars.2009.2541
35. Eastman RT, Fidock DA. Artemisinin-based combination therapies: a vital tool in efforts to eliminate malaria. Nat Rev Microbiol 2009; 7:864-74; PMID:19881520
36. Anvikar AR, Sharma B, Shahi BH, Tyagi PK, Bose TK, Sharma SK, Srivastava P, Srivastava B, Kiechel JR, Dash AP, et al. Artesunate-amodiaquine fixed dose combination for the treatment of Plasmodium falciparum malaria in India. Malar J 2012; 11:97; PMID:22458860; http://dx.doi.org/10.1186/1475-2875-11-97
37. Lamore SD, Azimian S, Horn D, Anglin BL, Uchida K, Cabello CM, Wondrak GT. The malondialdehyde-derived fluorophore DHP-lysine is a potent sensitizer of UVA-induced photooxidative stress in human skin cells. J Photochem Photobiol B 2010; 101:251-64; PMID:20724175; http://dx.doi.org/10.1016/j.jphotobiol.2010.07.010
38. Lamore SD, Qiao S, Horn D, Wondrak GT. Proteomic identification of cathepsin B and nucleophosmin as novel UVA-targets in human skin fibroblasts. Photochem Photobiol 2010; 86:1307-17; PMID:20946361; http://dx.doi.org/10.1111/j.1751-1097.2010.00818.x
39. Eskelinen E-L. Roles of LAMP-1 and LAMP-2 in lysosome biogenesis and autophagy. Mol Aspects Med 2006; 27:495-502; PMID:16973206; http://dx.doi.org/10.1016/j.mam.2006.08.005
40. Mizushima N, Yoshimori T. How to interpret LC3 immunoblotting. Autophagy 2007; 3:542-5; PMID:17611390
41. Ichimura Y, Kominami E, Tanaka K, Komatsu M. Selective turnover of p62/A170/SQSTM1 by autophagy. Autophagy 2008; 4:1063-6; PMID:18776737
42. Johansen T, Lamark T. Selective autophagy mediated by autophagic adapter proteins. Autophagy 2011; 7:279-96; PMID:21189453; http://dx.doi.org/10.4161/auto.7.3.14487
43. Pankiv S, Clausen TH, Lamark T, Brech A, Bruun JA, Outzen H, Øvervatn A, Bjørkøy G, Johansen T. p62/SQSTM1 binds directly to Atg8/LC3 to facilitate degradation of ubiquitinated protein aggregates by autophagy. J Biol Chem 2007; 282:24131-45; PMID:17580304; http://dx.doi.org/10.1074/jbc.M702824200
44. Kabuta T, Furuta A, Aoki S, Furuta K, Wada K. Aberrant interaction between Parkinson disease-associated mutant UCH-L1 and the lysosomal receptor for chaperone-mediated autophagy. J Biol Chem 2008; 283:23731-8; PMID:18550537; http://dx.doi.org/10.1074/jbc.M801918200
45. Sevlever D, Jiang P, Yen SH. Cathepsin D is the main lysosomal enzyme involved in the degradation of alpha-synuclein and generation of its carboxy-terminally truncated species. Biochemistry 2008; 47:9678-87; PMID:18702517; http://dx.doi.org/10.1021/bi800699v
46. Wang J. Beclin 1 bridges autophagy, apoptosis and differentiation. Autophagy 2008; 4:947-8; PMID:18769161
47. Maggs JL, Tingle MD, Kitteringham NR, Park BK. Drug-protein conjugates--XIV. Mechanisms of formation of protein-arylating intermediates from amodiaquine, a myelotoxin and hepatotoxin in man. Biochem Pharmacol 1988; 37:303-11; PMID:3342086; http://dx.doi.org/10.1016/0006-2952(88)90733-2
48. Tafazoli S, O'Brien PJ. Amodiaquine-induced oxidative stress in a hepatocyte inflammation model. Toxicology 2009; 256:101-9; PMID:19059302; http://dx.doi.org/10.1016/j.tox.2008.11.006
49. Mizushima N, Yoshimori T, Levine B. Methods in mammalian autophagy research. Cell 2010; 140:313-26; PMID:20144757; http://dx.doi.org/10.1016/j.cell.2010.01.028
50. Yamamoto A, Tagawa Y, Yoshimori T, Moriyama Y, Masaki R, Tashiro Y. Bafilomycin A1 prevents maturation of autophagic vacuoles by inhibiting fusion between autophagosomes and lysosomes in rat hepatoma cell line, H-4-II-E cells. Cell Struct Funct 1998; 23:33-42; PMID:9639028; http://dx.doi.org/10.1247/csf.23.33
51. Marceau F, Bawolak MT, Lodge R, Bouthillier J, Gagné-Henley A, Gaudreault RC, Morissette G. Cation trapping by cellular acidic compartments: beyond the concept of lysosomotropic drugs. Toxicol Appl Pharmacol 2012; 259:1-12; PMID:22198553; http://dx.doi.org/10.1016/j.taap.2011.12.004
52. Homewood CA, Warhurst DC, Peters W, Baggaley VC. Lysosomes, pH and the anti-malarial action of chloroquine. Nature 1972; 235:50-2; PMID:4550396; http://dx.doi.org/10.1038/235050a0
53. Slater AF. Chloroquine: mechanism of drug action and resistance in Plasmodium falciparum. Pharmacol Ther 1993; 57:203-35; PMID:8361993; http://dx.doi.org/10.1016/0163-7258(93)90056-J
54. Koike M, Shibata M, Waguri S, Yoshimura K, Tanida I, Kominami E, Gotow T, Peters C, von Figura K, Mizushima N, et al. Participation of autophagy in storage of lysosomes in neurons from mouse models of neuronal ceroid-lipofuscinoses (Batten disease). Am J Pathol 2005; 167:1713-28; PMID:16314482; http://dx.doi.org/10.1016/S0002-9440(10)61253-9
55. Ha SD, Ham B, Mogridge J, Saftig P, Lin S, Kim SO. Cathepsin B-mediated autophagy flux facilitates the anthrax toxin receptor 2-mediated delivery of anthrax lethal factor into the cytoplasm. J Biol Chem 2010; 285:2120-9; PMID:19858192; http://dx.doi.org/10.1074/jbc.M109.065813
56. Boya P, Gonzalez-Polo RA, Poncet D, Andreau K, Vieira HL, Roumier T, Perfettini JL, Kroemer G. Mitochondrial membrane permeabilization is a critical step of lysosome-initiated apoptosis induced by hydroxychloroquine. Oncogene 2003; 22:3927-36; PMID:12813466; http://dx.doi.org/10.1038/sj.onc.1206622
57. Fantin VR, Berardi MJ, Scorrano L, Korsmeyer SJ, Leder P. A novel mitochondriotoxic small molecule that selectively inhibits tumor cell growth. Cancer Cell 2002; 2:29-42; PMID:12150823; http://dx.doi.org/10.1016/S1535-6108(02)00082-X
58. Fantin VR, Leder P. Mitochondriotoxic compounds for cancer therapy. Oncogene 2006; 25:4787-97; PMID:16892091; http://dx.doi.org/10.1038/sj.onc.1209599
59. Cabello CM, Lamore SD, Bair WB 3rd, Davis AL, Azimian SM, Wondrak GT. DCPIP (2,6-dichlorophenolindophenol) as a genotype-directed redox chemotherapeutic targeting NQO1*2 breast carcinoma. Free Radic Res 2011; 45:276-92; PMID:21034357; http://dx.doi.org/10.3109/10715762.2010.526766
60. Gartel AL, Radhakrishnan SK. Lost in transcription: p21 repression, mechanisms, and consequences. Cancer Res 2005; 65:3980-5; PMID:15899785; http://dx.doi.org/10.1158/0008-5472.CAN-04-3995
61. Davis AL, Cabello CM, Qiao S, Azimian S, Wondrak GT. Phenotypic identification of the redox dye methylene blue as an antagonist of heat shock response gene expression in metastatic melanoma cells. Int J Mol Sci 2013; 14:4185-202; PMID:23429201; http://dx.doi.org/10.3390/ijms14024185
62. Qiao S, Lamore SD, Cabello CM, Lesson JL, Muñoz-Rodriguez JL, Wondrak GT. Thiostrepton is an inducer of oxidative and proteotoxic stress that impairs viability of human melanoma cells but not primary melanocytes. Biochem Pharmacol 2012; 83:1229-40; PMID:22321511; http://dx.doi.org/10.1016/j.bcp.2012.01.027
63. Luo J, Solimini NL, Elledge SJ. Principles of cancer therapy: oncogene and non-oncogene addiction. Cell 2009; 136:823-37; PMID:19269363; http://dx.doi.org/10.1016/j.cell.2009.02.024
64. Qiao S, Cabello CM, Lamore SD, Lesson JL, Wondrak GT. D-Penicillamine targets metastatic melanoma cells with induction of the unfolded protein response (UPR) and Noxa (PMAIP1)-dependent mitochondrial apoptosis. Apoptosis 2012; 17:1079-94; PMID:22843330; http://dx.doi.org/10.1007/s10495-012-0746-x
65. Cabello CM, Bair WB 3rd, Ley S, Lamore SD, Azimian S, Wondrak GT. The experimental chemotherapeutic N6-furfuryladenosine (kinetin-riboside) induces rapid ATP depletion, genotoxic stress, and CDKN1A(p21) upregulation in human cancer cell lines. Biochem Pharmacol 2009; 77:1125-38; PMID:19186174; http://dx.doi.org/10.1016/j.bcp.2008.12.002
66. Warfel NA, El-Deiry WS. p21WAF1 and tumourigenesis: 20 years after. Curr Opin Oncol 2013; 25:52-8; PMID:23159848; http://dx.doi.org/10.1097/CCO.0b013e32835b639e
67. Ma Y, Kurtyka CA, Boyapalle S, Sung SS, Lawrence H, Guida W, Cress WD. A small-molecule E2F inhibitor blocks growth in a melanoma culture model. Cancer Res 2008; 68:6292-9; PMID:18676853; http://dx.doi.org/10.1158/0008-5472.CAN-08-0121
68. DeGregori J, Johnson DG. Distinct and Overlapping Roles for E2F Family Members in Transcription, Proliferation and Apoptosis. Curr Mol Med 2006; 6:739-48; PMID:17100600
69. Biswas AK, Johnson DG. Transcriptional and nontranscriptional functions of E2F1 in response to DNA damage. Cancer Res 2012; 72:13-7; PMID:22180494; http://dx.doi.org/10.1158/0008-5472.CAN-11-2196
70. Samant GV, Wali VB, Sylvester PW. Anti-proliferative effects of gamma-tocotrienol on mammary tumour cells are associated with suppression of cell cycle progression. Cell Prolif 2010; 43:77-83; PMID:19922488; http://dx.doi.org/10.1111/j.1365-2184.2009.00657.x
71. Macdonald JI, Dick FA. Posttranslational modifications of the retinoblastoma tumor suppressor protein as determinants of function. Genes Cancer 2012; 3:619-33; PMID:23634251; http://dx.doi.org/10.1177/1947601912473305
72. Wibo M, Poole B. Protein degradation in cultured cells. II. The uptake of chloroquine by rat fibroblasts and the inhibition of cellular protein degradation and cathepsin B1. J Cell Biol 1974; 63:430-40; PMID:4607946; http://dx.doi.org/10.1083/jcb.63.2.430
73. Klionsky DJ, Abdalla FC, Abeliovich H, Abraham RT, Acevedo-Arozena A, Adeli K, Agholme L, Agnello M, Agostinis P, Aguirre-Ghiso JA, et al. Guidelines for the use and interpretation of assays for monitoring autophagy. Autophagy 2012; 8:445-544; PMID:22966490; http://dx.doi.org/10.4161/auto.19496

74. Maclean KH, Dorsey FC, Cleveland JL, Kastan MB. Targeting lysosomal degradation induces p53-dependent cell death and prevents cancer in mouse models of lymphomagenesis. J Clin Invest 2008; 118:79-88; PMID:18097482; http://dx.doi.org/10.1172/JCI33700
75. Zhu H, Zhang L, Wu S, Teraishi F, Davis JJ, Jacob D, Fang B. Induction of S-phase arrest and p21 overexpression by a small molecule 2[[3-(2,3-dichlorophenoxy)propyl] amino]ethanol in correlation with activation of ERK. Oncogene 2004; 23:4984-92; PMID:15122344; http://dx.doi.org/10.1038/sj.onc.1207645
76. Ogryzko VV, Wong P, Howard BH. WAF1 retards S-phase progression primarily by inhibition of cyclin-dependent kinases. Mol Cell Biol 1997; 17:4877-82; PMID:9234744
77. Joe AK, Liu H, Suzui M, Vural ME, Xiao D, Weinstein IB. Resveratrol induces growth inhibition, S-phase arrest, apoptosis, and changes in biomarker expression in several human cancer cell lines. Clin Cancer Res 2002; 8:893-903; PMID:11895924
78. Knudsen KE, Booth D, Naderi S, Sever-Chroneos Z, Fribourg AF, Hunton IC, Feramisco JR, Wang JY, Knudsen ES. RB-dependent S-phase response to DNA damage. Mol Cell Biol 2000; 20:7751-63; PMID:11003670; http://dx.doi.org/10.1128/MCB.20.20.7751-7763.2000
79. Hockenbery DM. Targeting mitochondria for cancer therapy. Environ Mol Mutagen 2010; 51:476-89; PMID:20213841; http://dx.doi.org/10.1002/em.20552
80. Maycotte P, Aryal S, Cummings CT, Thorburn J, Morgan MJ, Thorburn A. Chloroquine sensitizes breast cancer cells to chemotherapy independent of autophagy. Autophagy 2012; 8:200-12; PMID:22252008; http://dx.doi.org/10.4161/auto.8.2.18554
81. Neckers L, Workman P. Hsp90 molecular chaperone inhibitors: are we there yet? Clin Cancer Res 2012; 18:64-76; PMID:22215907; http://dx.doi.org/10.1158/1078-0432.CCR-11-1000
82. Wang RE. Targeting heat shock proteins 70/90 and proteasome for cancer therapy. Curr Med Chem 2011; 18:4250-64; PMID:21838681; http://dx.doi.org/10.2174/092986711797189574
83. Ochong EO, van den Broek IV, Keus K, Nzila A. Short report: association between chloroquine and amodiaquine resistance and allelic variation in the *Plasmodium falciparum* multiple drug resistance 1 gene and the chloroquine resistance transporter gene in isolates from the upper Nile in southern Sudan. Am J Trop Med Hyg 2003; 69:184-7; PMID:13677373
84. Famin O, Ginsburg H. Differential effects of 4-aminoquinoline-containing antimalarial drugs on hemoglobin digestion in Plasmodium falciparum-infected erythrocytes. Biochem Pharmacol 2002; 63:393-8; PMID:11853690; http://dx.doi.org/10.1016/S0006-2952(01)00878-4
85. Obua C, Gustafsson LL, Aguttu C, Anokbonggo WW, Ogwal-Okeng JW, Chiria J, Hellgren U. Improved efficacy with amodiaquine instead of chloroquine in sulfadoxine/pyrimethamine combination treatment of falciparum malaria in Uganda: experience with fixed-dose formulation. Acta Trop 2006; 100:142-50; PMID:17113554; http://dx.doi.org/10.1016/j.actatropica.2006.10.007
86. Hawley SR, Bray PG, Park BK, Ward SA. Amodiaquine accumulation in *Plasmodium falciparum* as a possible explanation for its superior antimalarial activity over chloroquine. Mol Biochem Parasitol 1996; 80:15-25; PMID:8885219; http://dx.doi.org/10.1016/0166-6851(96)02655-2
87. Mirković B, Sosič I, Gobec S, Kos J. Redox-based inactivation of cysteine cathepsins by compounds containing the 4-aminophenol moiety. PLoS One 2011; 6:e27197; PMID:22073285; http://dx.doi.org/10.1371/journal.pone.0027197
88. Parikh S, Ouedraogo JB, Goldstein JA, Rosenthal PJ, Kroetz DL. Amodiaquine metabolism is impaired by common polymorphisms in CYP2C8: implications for malaria treatment in Africa. Clin Pharmacol Ther 2007; 82:197-203; PMID:17361129; http://dx.doi.org/10.1038/sj.clpt.6100122
89. Roederer MW, McLeod H, Juliano JJ. Can pharmacogenomics improve malaria drug policy? Bull World Health Organ 2011; 89:838-45; PMID:22084530; http://dx.doi.org/10.2471/BLT.11.087320
90. Lamore SD, Cabello CM, Wondrak GT. The topical antimicrobial zinc pyrithione is a heat shock response inducer that causes DNA damage and PARP-dependent energy crisis in human skin cells. Cell Stress Chaperones 2010; 15:309-22; PMID:19809895; http://dx.doi.org/10.1007/s12192-009-0145-6
91. Werle B, Ebert W, Klein W, Spiess E. Assessment of cathepsin L activity by use of the inhibitor CA-074 compared to cathepsin B activity in human lung tumor tissue. Biol Chem Hoppe Seyler 1995; 376:157-64; PMID:7612192; http://dx.doi.org/10.1515/bchm3.1995.376.3.157
92. Levicar N, Dewey RA, Daley E, Bates TE, Davies D, Kos J, Pilkington GJ, Lah TT. Selective suppression of cathepsin L by antisense cDNA impairs human brain tumor cell invasion in vitro and promotes apoptosis. Cancer Gene Ther 2003; 10:141-51; PMID:12536203; http://dx.doi.org/10.1038/sj.cgt.7700546